Phase Contrast Cine Magnetic Resonance Imaging

Article *in* Magnetic resonance quarterly · November 1991

Source: PubMed

4 authors, including:

Norbert J Pelc
Stanford University
372 PUBLICATIONS **13,460** CITATIONS

SEE PROFILE

Robert J Herfkens
Stanford University
281 PUBLICATIONS **10,642** CITATIONS

SEE PROFILE

Dieter R Enzmann
University of California, Los Angeles
130 PUBLICATIONS **5,977** CITATIONS

SEE PROFILE

Magnetic Resonance Quarterly
Vol. 7, No. 4, pp. 229–254

Phase Contrast Cine Magnetic Resonance Imaging

Norbert J. Pelc, Robert J. Herfkens, *Ann Shimakawa, and Dieter R. Enzmann

*Department of Radiology, Stanford University School of Medicine, Stanford, California, and *GE Medical Systems, Waukesha, Wisconsin, U.S.A.*

Abstract: Phase contrast cine magnetic resonance imaging (MRI) combines the flow-dependent contrast of phase contrast MRI with the ability of cardiac cine imaging to produce images throughout the cardiac cycle. Two pulse sequence types are used for sensitivity to flow in one direction, whereas four are needed for sensitivity in all directions. Several alternatives for synchronization of the data to the cardiac cycle exist. Retrospectively interpolated methods can image the entire cardiac cycle efficiently. Rapid interleaving of the various sequence types ensures immunity to motion misregistration. The technique produces images in which contrast is related to flow velocity as well as magnitude images such as those of conventional cine MRI. The data can be interpreted qualitatively to demonstrate the presence, magnitude, and direction of flow, and quantitatively to provide estimates of flow velocity, volume flow rate, and displaced volumes. Phase contrast cine MRI is helpful in the diagnosis of aortic dissections, in the study of flow distributions in large vessels such as pulmonary arteries, as well as in smaller vessels such as carotid and basilar arteries, and in the evaluation of complex anatomical variants. Future developments are expected to reduce imaging time and expand the quantitative applications. **Key Words:** Magnetic resonance imaging—Phase contrast—Flow—Cardiac cine.

Magnetic resonance imaging (MRI) has been shown to be a valuable tool for the noninvasive assessment of the cardiovascular system. The early success with spin-echo (SE) imaging was largely based on the high contrast between the dark appearance of flowing blood and higher signal from static structures in these images (1).

Rapid gradient-echo imaging, in which smoothly flowing blood demonstrates relatively high signal intensity, provides a flow-dependent contrast mechanism and efficient utilization of imaging time. Cine MRI (2) using short repetition time (TR) gradient-echo sequences and some form of cardiac synchronization is useful for imaging dynamic processes (3–6). It provides some information about the presence of flow due to inflow enhancement. However, this flow information is only qualitative because the signal intensity of flowing fluid has a complicated dependence on many factors, including echo delay, spatial resolution and slice thickness, flow direction, and relaxation times.

Phase contrast MRI refers to a family of MR imaging methods that exploit the fact that spins that move through magnetic field gradients obtain a different phase than static spins, enabling the production of images with controlled sensitivity to flow. Among the advantages of phase contrast MRI are its adjustable sensitivity to flow and, in some cases, the quantitative nature of the resulting data.

The combination of these two tools, phase contrast and cine MR, produces a technique, first described by Nayler et al. (7), that can depict motion

Address correspondence and reprint requests to Dr. N. J. Pelc at Department of Radiology, Stanford University School of Medicine, S-047, Stanford, CA 94305-5105, U.S.A.

and flow throughout the cardiac cycle. It can be used to qualitatively describe flow in complex situations and can also be used to quantitate flow velocities and volumes. This ability to noninvasively provide flow information in image form and without restrictions imposed by acoustic windows has significantly expanded the utility of MRI.

The purpose of this report is to describe the technical considerations in the method, to demonstrate the clinical areas in which phase contrast cine can be used, to discuss the quantitative use of the resulting data, and, finally, to suggest areas of further development.

TECHNICAL PRINCIPLES AND ALTERNATIVES

Fundamentals of phase contrast MRI

The fundamental sensitivity of the phase of the nuclear magnetic resonance signal to motion in the presence of magnetic field gradients was described by Hahn in 1960 (8), further refined by Singer et al. (9), and later extended to MRI (10). Each MRI raw data set produces an image that portrays the transverse magnetization in each voxel. This transverse magnetization is a vector quantity having both magnitude and direction (phase). Typically, in MRI only the magnitude of the magnetization contributes to the image intensity. However, the phase can contain information about motion. As is shown in the Appendix, motion in the presence of a magnetic field gradient produces a change in phase proportional to velocity v:

$$\phi = v\,(\gamma M_1) \tag{1}$$

where γ is the gyromagnetic ratio and M_1 is the first moment of the gradient waveform $G(t)$ evaluated at the echo delay time (TE):

$$M_1 = \int_0^{TE} G(t)\, t\, dt. \tag{2}$$

In a manner completely analogous to spatial phase encoding for image generation, measurements made with a large number of values of M_1 phase encode in the flow velocity direction. Fourier transformation of the measurements as functions of M_1 separates the signal in each spatial resolution element into components with different velocities in the direction of M_1 (10,11). For a given degree of spatial localization, this approach imposes a large (i.e., 128-fold) increase in scan time. It is presently being pursued for applications in which the dimensions of spatial localization are reduced so as to maintain an acceptable imaging time (12,13). These are powerful techniques, but they will not be discussed further here. Rather, we assume that the spins in a voxel are moving similarly and can be well described by an average velocity v. As a result, the task is much simpler than having to characterize the distribution of velocities in a voxel; we need only estimate a single velocity parameter for each voxel.

Imaging gradients typically have nonzero first moments (unless moment nulling is used) and therefore, perhaps inadvertently, sensitize the data to motion. Van Dijk (14) showed that the read-out gradient waveform encodes motion in the direction of this gradient into the phase of the signal, and demonstrated the effect of flow and myocardial motion in spin-echo data. Bryant et al. showed that flow in the slice direction could be measured with spin-echo sequences (15). The difficulty with these methods, which rely on a single phase measurement for each voxel, is that the phase can easily be affected by superfluous sources, such as velocities in directions other than the one being studied, pulse sequence timing errors, and radiofrequency effects. However, the gradient waveform can be modified to alter the first moment (motion sensitivity) while maintaining the same image localization characteristics. Images acquired with this altered waveform will contain most if not all of the unwanted phase effects but will have a different phase shift due to motion. If two complete data sets are acquired with gradient waveforms that have a different first moment in one direction, the difference in phase in each pixel will be

$$\Delta\phi = v\,(\gamma \Delta M_1) \tag{3}$$

Static structures will exhibit no phase change. By acquiring two measurements with different gradient first moments, the method can be sensitive to phase shifts due to motion yet be insensitive to other phase effects. Essentially, the image produced by one acquisition acts as a phase reference for the image acquired with modified flow sensitivity due to the altered gradient waveform.

Early implementations of this phase difference approach used spin-echo sequences (16), which are not well suited for blood flow studies since they tend to exhibit low intraluminal signal. Gradient-echo phase contrast methods (7,17,18) are preferred and are used almost exclusively for such work. Use

of two measurements rather than one is particularly important when gradient-echo sequences are used because magnetic field inhomogeneity produces large phase shifts.

Encoding strategies

To sensitize the data to motion in one direction and yet be insensitive to other phase effects, measurements with two sequence types (pulse sequences with different gradient first moments) are needed. One approach for this is shown in Fig. 1. The sequence in Fig. 1A is flow compensated (first moment nulled) in the slice and read directions, and has a phase-encoding rewinder after signal acquisition to maintain the steady-state equilibrium (2). After data are collected with all the spatial phase-encoding amplitudes (only one of which is shown), an image in which each pixel is a complex quantity can be produced. The magnitude (or modulus) of the complex image is a flow-compensated gradient-recalled acquisition in a steady state (GRASS) image. The phase of this image contains effects due to magnetic field inhomogeneity, pulse sequence timing, and so forth.

To encode motion in one direction, the gradient first moment in the desired direction must be altered. This could be done by adding a bipolar lobe to the appropriate gradient waveform to shift the phase of moving spins (10). A more efficient approach combines the roles of flow encoding and imaging into three lobes, as shown in Fig. 1B. For example, if flow in the slice-select direction is of interest, the waveforms for the readout and phase-encoded directions are left unchanged (solid lines) but the last two lobes of the slice-select gradient are modified to the dashed curves. Because the dashed and solid waveforms have equal total area, static spins are unaffected by the change. However, because the first moment is changed as compared with that in Fig. 1A, spins moving in the slice-select direction will obtain an incremental phase. When the data are reconstructed and the phase of the resulting image is subtracted from that of Fig. 1A, an image is obtained in which pixel values are dependent on motion in the slice-select direction. If sensitivity to motion in the phase-encoded direction is desired, the original (solid) slice and read direction waveforms are used and a bipolar lobe (dashed) is added to the gradient waveform in the phase-encoded direction. Similarly, for sensitivity to motion in the readout direction, the first two lobes of the readout gradient waveform are altered.

The critical difference between the two sequences is the first moment in the direction of interest. In the example shown in Fig. 1, one sequence is moment nulled ($M_1 = 0$) and the other is flow encoded ($M_1 = \Delta M_1$). Two-sided encoding acquires data with measurements symmetric about $M_1 = 0$, one sequence with $M_1 = -\Delta M_1/2$ and the other with $M_1 = \Delta M_1/2$. In another approach, first moments are centered about an offset selected to minimize echo delay. In simple situations, the phase difference images produced by these methods are identical, but the results from these techniques may differ when voxels contain a wide range of velocities and when the velocity is not consistent among sequence repetitions.

Two sequence types are needed to image flow in one direction. If the gradient first moments in two directions are altered in the two sequences, the measurement will simply reflect velocity in the vector sum of the two directions. Four sequence types are needed to image all three velocity components. A simple four-point method uses a single reference

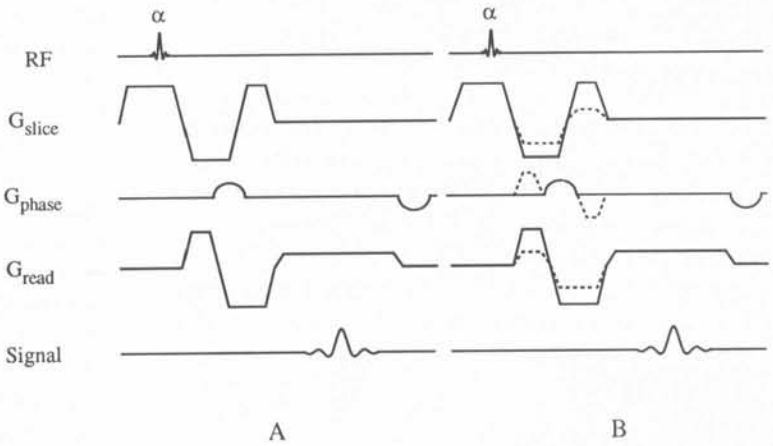

FIG. 1. Phase contrast gradient echo pulse sequence. **A:** A first-order moment nulled GRASS sequence. **B:** For acquisition of data sensitive to motion in one direction, a second data set is acquired with the gradient waveform along one of the gradient axes changed from the solid line to the dashed line.

sequence and three differentially encoded ones (19,20). For example, the reference sequence might be flow compensated, as in Fig. 1A. The three other sequence types would have modified waveforms for one spatial axis. Subtraction of the first sequence's phase image from each of the others yields three phase difference images, one for each Cartesian direction. Two-sided encoding (i.e., $M_1 = \pm \Delta M_1/2$) of flow in all directions can be performed with a reference measurement having a nonzero first moment in each direction. An alternate four-point method imposes flow encoding along pairs of directions. This method has some interesting properties, and the interested reader is referred to an earlier work (19) for further details. With either of these encoding methods, three direction-dependent images are produced, one for each Cartesian direction. From these, an image equal to the square root of the sum of the squares of the three corresponding single direction images can be produced. In these speed images, structures with flow appear bright, with relative brightness dependent on speed but independent of direction.

Flow-encoding strength and signal-to-noise ratio

A critical parameter of phase contrast images is the strength of the flow encoding controlled by ΔM_1. This can be characterized by the phase change per unit velocity, $\gamma \Delta M_1$ with units of, for example, radians/cm/s. An intuitive alternative is the velocity, v_{enc}, that produces a phase shift of π radians or 180°:

$$v_{enc} = \pi/(\gamma \Delta M_1) \tag{4}$$

This parameter is useful because it also represents the largest speed that can be measured unambiguously. A velocity of $(1.1)v_{enc}$ will produce a phase shift of (1.1)180 = 198°. However, phase is only unique over a 360° range, and a phase shift of 198° is not distinguishable from a phase shift of −162°, and, therefore, neither are velocities of $(1.1)v_{enc}$ and $(-0.9)v_{enc}$. This phenomenon is sometimes referred to as velocity aliasing and is analogous to spatial wraparound artifacts in MRI. Velocity aliasing can be reduced by use of algorithms that use spatial continuity to resolve the ambiguity (21). Without such algorithms, only velocities in the range of $-v_{enc}$ to v_{enc} can be imaged unambiguously, and the measured phase shift is converted to velocity by

$$v = \left(\frac{v_{enc}}{\pi}\right) \Delta\phi. \tag{5}$$

The signal-to-noise ratio (SNR) of this measurement depends on the noise in the phase measurements and on the flow sensitivity (19). The SNR of the measured velocity, SNR_v, is

$$SNR_v = \left(\frac{\pi}{\sqrt{2}}\right)\left(\frac{v}{v_{enc}}\right) SNR, \tag{6}$$

where SNR is the SNR in a single acquired image. The $\sqrt{2}$ penalty results from the subtraction operation. SNR_v increases with decreasing v_{enc} and with increasing SNR. The latter underscores the advantage of using sequences with high intraluminal signal, such as gradient-echo methods, for vascular applications.

Gating alternatives

To resolve changes in flow throughout the cardiac cycle, measurements are needed with each sequence type (2 or 4) at each point in the cardiac cycle. Alternatives exist for how the synchronization to the cardiac cycle is performed, such as prospective triggering versus retrospective gating, as well as for the degree of sequence type interleaving.

The earliest gated phase contrast methods (7) are best described as multiphase cardiac triggered. With knowledge of the patient's heart rate and the sequence TR, an estimate is made of the number of sequences that fit in one cardiac period. A train of sequences is triggered upon detection of the beginning of a cardiac cycle, all with the same phase-encoding amplitude. This is repeated with a different phase-encoding amplitude in subsequent cycles to produce complete data sets. This method has two disadvantages stemming from beat-to-beat variations in the length of the cardiac cycle. One disadvantage is that the first sequence in the cycle is preceded by a longer (and variable) relaxation period than the others. This disrupts the NMR equilibrium and causes flashing artifacts in the first few frames (2). The second disadvantage results from the fact that the number of sequences per cycle is typically selected to occupy less than the entire cardiac period and thereby ensure that the next period is not missed. As a result, this method has difficulty examining the entire cycle. This can be somewhat improved by purposely selecting a number of cycles that will exceed one period. Whereas the entire cycle is then covered, the scan time is greatly lengthened and variation in the cardiac rate will temporally blur the late frames.

An alternate gating strategy acquires data at a constant rate and retrospectively sorts and interpolates the data into the desired number of frames per cycle (2). The term cine MRI or cine will be used here to refer to such techniques. As originally described, sequence executions proceed at a constant rate and with a constant phase-encoding amplitude within each cardiac period (Fig. 2A). The phase-encoding amplitude is incremented upon detection of the beginning of a new cycle, and the temporal location within each cardiac cycle of each sequence is recorded. After the data are acquired, raw data interpolation is used to produce consistent data for the desired number of cardiac frames. Because sorting and interpolation are retrospective, the entire cardiac cycle is examined and the frames at the end of the cycle are as well time resolved as those at the beginning. Use of a constant TR enables this method to avoid flashing artifacts. A fully retrospective cine MRI method has been described (22). In this method a number of sequences that is guaranteed to cover more than one complete cycle are executed at each phase-encoding amplitude (Fig. 2B), and either a simultaneously recorded electrocardiogram (ECG) or the NMR data itself are retrospectively used to assign a location in the cycle to each acquired echo. Again, interpolation is used to produce the desired number of frames. The scan time is somewhat longer than for the method that uses real-time phase-encoding selection, but this method is easier to implement and may be more resistant to abnormal triggers. With either of these cine methods, the asynchronous nature of sequence executions causes the temporal resolution at the beginning of the cycle to be somewhat worse than in the cardiac-triggered method.

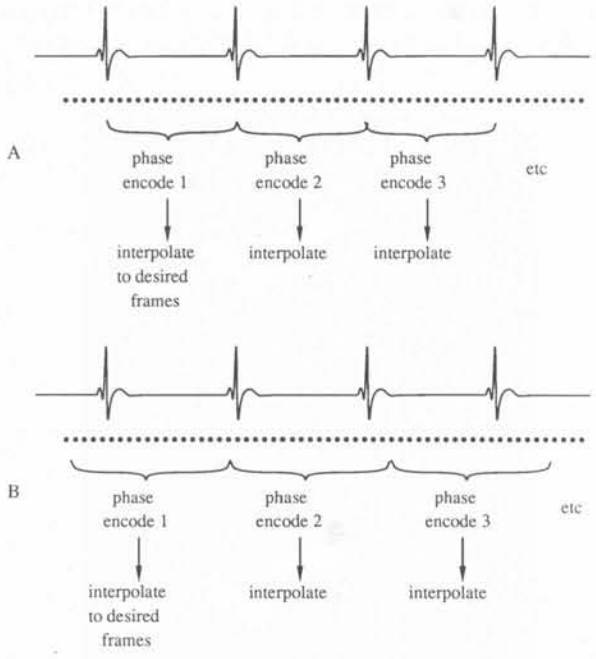

FIG. 2. A: In one form of cine MRI, all of the sequences in one cardiac period use the same phase-encoding amplitude, and the phase encoding is selected in real time. B: In fully retrospective cine, a set of sequences known to cover at least one cardiac period use the same phase-encoding amplitude. In both, interpolation is used to generate data for the desired number of frames in the cycle from the data acquired with the same phase encoding.

The degree of interleaving of the various sequence types affects the sensitivity of the method to motion artifacts. At one extreme, an entire raw data set can be acquired with one sequence type followed by another (one or three) scan with modified flow sensitivity. This is the easiest method to implement but the most sensitive to misregistration artifacts, because several minutes elapse between the acquisition of the various data sets. A better approach is to alternate flow sensitivity in adjacent cardiac periods. For example, for sensitivity to flow in one direction, data are collected during an entire cycle with the sequence of Fig. 1A, and in the next cardiac period data are collected with the same phase-encoding amplitude but with the sequence of Fig. 1B. Relatively slow motion will produce common changes in the two data sets and will be suppressed in the subtraction process.

We have found considerably improved immunity to motion artifacts when interleaving is performed within each cardiac cycle, as shown in Fig. 3A and B for sensitivity in one and all directions, respectively (23). The data collected with each sequence type are separately sorted and interpolated into the desired number of frames per cycle. Temporal offsets between the data sets are corrected at this step. Whereas this method of interleaving offers the most immunity to motion artifacts, it degrades the temporal resolution by a factor of two or four as compared with the other techniques. On the other hand, the minimum scan time is reduced by the same amount and use of short TR yields acceptable temporal resolution. The interleaving scheme of Fig. 3B can also be used to image flow in one direction in two physical slices simultaneously at the expense of temporal resolution.

Data processing alternatives

Data acquisition produces two or four raw data sets, each producing a magnitude and a phase im-

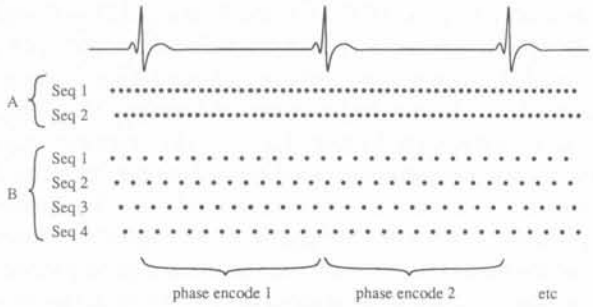

FIG. 3. Measurements with the various sequence types are interleaved within each cardiac cycle. Sequences in the same cycle have the same spatial phase encoding, and the phase encoding is switched when a new cycle is detected. A: Interleaving of two sequence types (sequences 1 and 2) for imaging flow in one direction in one slice. B: Interleaving of four sequence types for imaging all three flow components. These sequences can also be used to image one component of flow in two slices, in which case sequences 1 and 3 would interrogate one slice with different first moments, whereas sequences 2 and 4 would interrogate the other slice.

age, and there are several alternatives in the way these data can be combined.

If the encoding strategy of Fig. 1 is used, the magnitude images from the first sequence (Fig. 1A) are exactly equivalent to conventional cine MRI images. Magnitude images from Fig. 1B are expected to have more flow artifacts due to the nonzero first moment. However, because the images are gated and the first moment is selected to maintain relatively consistent phase shifts within a voxel, the magnitude images from the two sequences are similar. In particular, as shown in Fig. 4, the image quality of the average of the magnitude images from the two acquisitions is better than that of the flow-compensated sequence alone (i.e., the noise reduction from averaging overcomes any artifact increase). Of course, the averaging must be performed on the magnitude images after Fourier transformation to ignore the phase shifts in the images. For acquisitions sensitized to flow in all directions, the magnitude images from the four data sets can be averaged.

If magnitude averaging is used, any deterministic difference between the magnitude images of the various sequences (flow compensated vs. flow encoded) should be viewed as a disadvantage. In these cases, use of two-sided flow encoding (i.e., $M_1 = \pm \Delta M_1/2$) should be considered, because the magnitude images will be produced with sequences having the same absolute value of the first moment, and therefore similar flow-related effects.

Velocity images can be formed by properly scaling the phase shift data (Eq. 5). One disadvantage of velocity images, shown in Fig. 5A, is that in regions of low signal intensity (and SNR), that is, outside

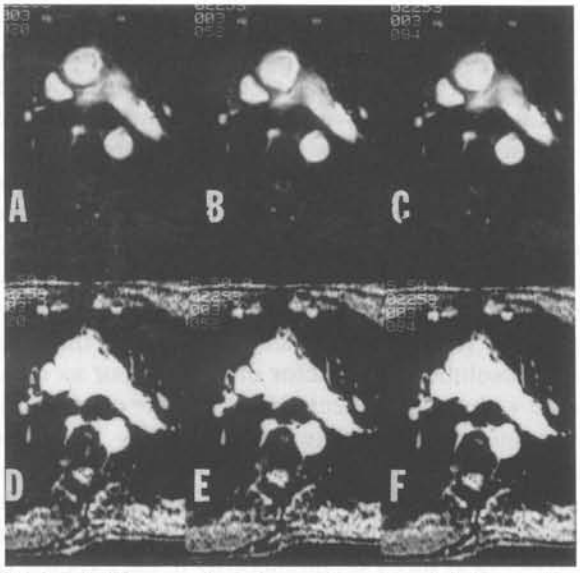

FIG. 4. A: The magnitude image at peak systole from a flow-compensated acquisition. B: The corresponding image from a flow-encoded acquisition (v_{enc} = 150 cm/s). D and E: The same images with a narrower window width. Intraluminal signal and flow related artifacts are comparable in magnitude reconstructions of the two data sets. C and F: The average of the two magnitude images.

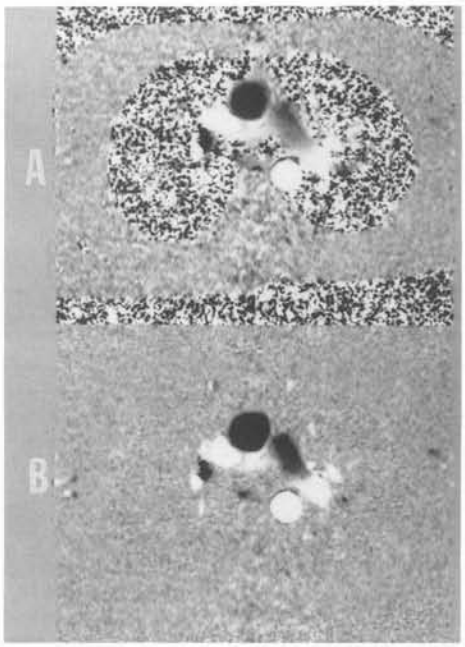

FIG. 5. A: Velocity image at peak systole has high noise level in areas where the NMR signal is low. B: This can be suppressed by multiplying the velocity image by the corresponding magnitude image (e.g., Fig. 4).

the object, the noise level is high (compare Eq. 6). Although these regions are typically not of interest diagnostically, the high noise level in them can be disturbing when the image is viewed. One solution is to suppress pixels in the velocity image if the magnitude in the pixel does not exceed some threshold. Another approach that does not require a priori selection of a threshold is to form an image in which the pixel value is the product of velocity and magnitude (Fig. 5B). In these magnitude-weighted or magnitude-masked images, noise in background regions is suppressed and vascular structures are enhanced due to their relative signal levels. As long as the magnitude images are retained, the weighting can be undone before, or as part of, any quantitative analysis.

Ideally, the observed phase shifts are due only to motion-induced effects. However, the measurements are made with altered gradient waveforms, and it is possible for eddy current effects to contribute to the measured effects. Note in Fig. 1 that most of the gradient lobes are common to the two measurements being subtracted. As a result, the only eddy currents that can influence the flow images are those due to the lobes being altered. With good eddy current compensation, and especially with shielded gradient coils, these effects are small, but are often observable as nonzero apparent velocities in structures known to be static. Due to the nature of their source, these velocity errors must be slowly varying across the image. Automated phase correction algorithms are available. A fairly simple one assumes that all apparent velocities that vary slowly across the image (e.g., constant or linear) must be artifactual. The algorithm estimates these components and subtracts them from the measured image. Unless the magnitude image is dominated by signal in flowing structures, these corrections are useful and reliable. However, they may not be sufficient for quantitative analyses (see below).

Summary

All of the various alternatives discussed here have not been compared exhaustively, and any results are expected to be application dependent. Nonetheless, an implementation that is routinely successful uses cine gating with real-time selection of phase-encoding amplitude, interleaving of the various sequence types within each cardiac cycle, two-sided encoding, magnitude averaging, and magnitude weighting. Except for applications where quantitative analysis is expected, automated phase correction is applied.

The data shown in Fig. 6 were acquired in a normal volunteer with flow encoding in the superior–inferior direction (v_{enc} = 150 cm/s), 256 × 128 matrix, 30 cm field of view, 5 mm slice thickness, two excitations, and respiratory compensation. Sixteen

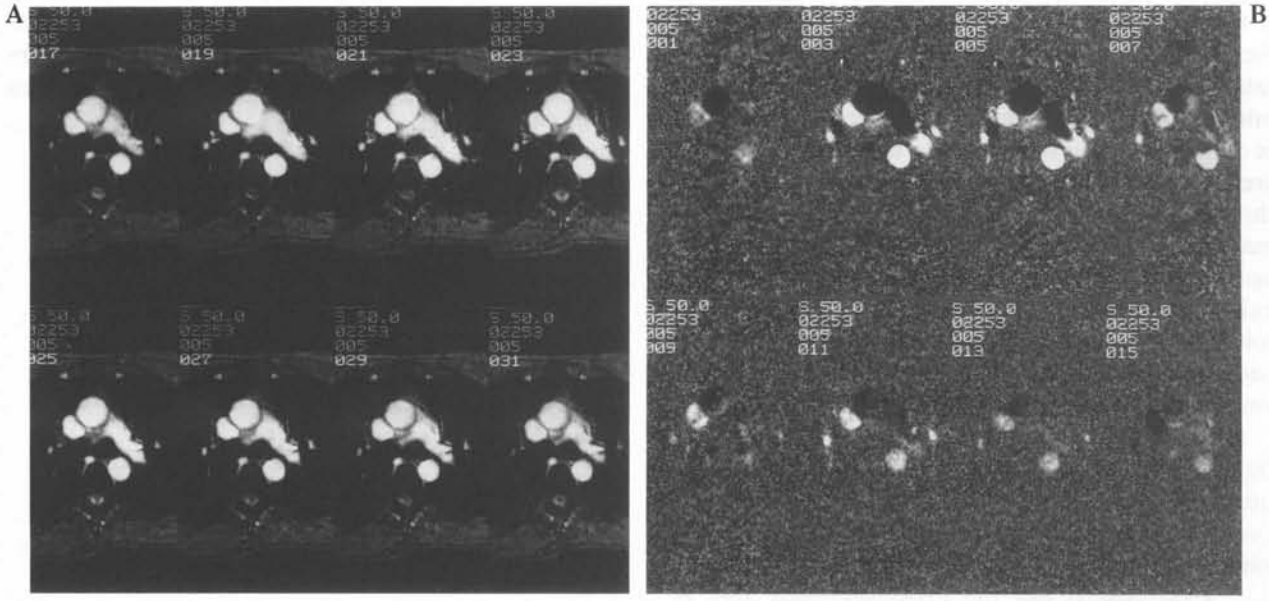

FIG. 6. Axial phase contrast cine images of a normal volunteer. A: Magnitude images for eight of 16 frames covering the entire cardiac cycle. B: Corresponding magnitude weighted velocity images. The data were encoded for flow in the cranio-caudal direction with caudally directed flow appearing bright and cranially directed motion displayed as dark pixels.

frames throughout the cycle were produced in a scan time of 4 min (256 heart beats, 67 bpm). Fig. 6A shows magnitude images for every other frame whereas Fig. 6B shows the corresponding magnitude weighted flow images. In Fig. 6B, static structures are grey, bright pixel values correspond to cranio-caudal flow, and dark pixel values correspond to flow in the reverse direction.

QUANTITATIVE ANALYSIS

For the case of homogeneous motion within a voxel, the phase shifts measured with the phase contrast technique can be used to estimate motion velocity (cm/s) in the direction of the flow-encoding gradient (Eq. 5). These velocity measurements can be used directly, much as Doppler measurements are. To estimate flow velocity with a two-point (single direction) technique, it is best to use an imaging plane that is perpendicular to the flow direction and to encode for through-slice motion. If the flow is oblique to the imaging plane (i.e., not parallel to the motion encoding direction), the flow velocity will be underestimated by a factor of $\cos(\Theta)$, where Θ is the angle between the flow direction and the motion-encoding direction. For reasonably small Θ, the error is small. Further, it may be possible to measure the angle of obliquity from acquired images and to correct for the underestimation by dividing by $\cos(\Theta)$. This correction works well for $\Theta \leq 45°$.

For through-plane flow, the product of the measured velocity (cm/s) and the pixel area (cm^2) is the rate of flow (ml/s) through the pixel. If a region of interest (ROI) that includes the entire vessel lumen is defined and the flow rates in the inscribed pixels are summed, an estimate of the volume flow rate through the vessel is obtained. This computation is mathematically equivalent to multiplying the average velocity within the ROI by the ROI area to calculate the flow rate. To first order, this method is tolerant to ROIs defined larger than the true lumen because the expected velocity in pixels outside the vessel boundary is zero (24,25).

As described already, if the flow is not parallel to the encoded direction, the velocity will be underestimated by $\cos(\Theta)$. However, it can be shown that even in these cases the volume flow rate is measured correctly (25,26). The velocity is underestimated by $\cos(\Theta)$ but the cross-sectional area is overestimated by $1/\cos(\Theta)$. Therefore, the product of the velocity at a pixel and the pixel area estimates the flow rate through the pixel independent of the exact flow direction. Fig. 7 shows the blood flow rate as a function of time in the ascending aorta, descending aorta, and superior vena cava computed from the data in Fig. 6.

The average throughout the cycle of the flow rate curve yields the average flow rate through a vessel. For the data in Fig. 7, the average flow rates in the ascending aorta, descending aorta, and SVC were 6.5, 4.8, and 2.8 L/min respectively. The product of the average flow rate and the cardiac period is the volume of flow through an ROI per cycle. Measurements in the aortic root can be used to estimate the left ventricular stroke volume (27). Using the ascending aorta measurement in Fig. 7, the left ventricular stroke volume was 98 ml. Other parameters than can be estimated include regurgitant flow and shunt volumes.

Whereas phase contrast flow rate measurements are tolerant to both excessively large ROI size and oblique flow, both effects should be minimized because as the ROI size increases (either directly or through angulation) the noise in the measurement will increase due to the additional pixels contributing to the result. Also, partial volume effects are not linear in phase measurements. This somewhat subtle effect can cause significant errors. Consider a voxel in which half of the volume contains static spins while the other half contains spins moving at a uniform velocity, and let the velocity-induced phase shift for these spins be ϕ_m. If the measured phase shift in the voxel is $\phi_m/2$, the voxel will contribute correctly to the total flow because the errors in the measured velocity and cross-sectional area will cancel.

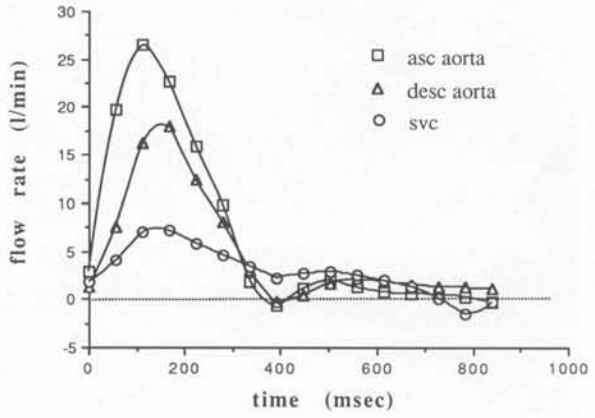

FIG. 7. Flow rate as a function of time in the ascending aorta, descending aorta, and superior vena cava computed from the data in Fig. 6.

Assume for now that the static and moving spins produce equal signal intensity. As shown in Fig. 8A, the measured signal is the vector sum of the signals from static and moving spins. Whereas the measured phase shift ϕ will be intermediate between ϕ_m and zero (the phase shift of the stationary spins), ϕ is not necessarily equal to $\phi_m/2$ because the arc tangent function is not linear. Thus, some errors may result, but for moderate ϕ_m these errors are small (24). However, due to inflow enhancement the moving spins can be responsible for a fraction of the total signal that is much larger than their volume fraction. Fig. 8B shows the case in which the moving spins contribute three times more signal per unit volume than static spins. In this case, even though the moving spins occupy only half the volume, they dominate the signal from the voxel. As a result, the measured phase shift will be much closer to ϕ_m and the flow rate through the voxel will be exaggerated. Thus, in the presence of inflow enhancement partial volume effects will cause the flow rate to be overestimated. These partial volume errors are minimized with the use of thin slices, small pixels, and imaging planes that are perpendicular to the flow direction.

As described earlier, eddy current effects from the flow-encoding gradients can cause undesired phase shifts. These phase errors add a bias to the measured velocity, which varies slowly across the image. Even though this velocity offset is generally a small fraction of the velocity dynamic range, it can cause significant errors in flow estimates when the ROI is large. The eddy current effects can be estimated by measuring the apparent velocity in regions known to be static, and subtracting the error from the pixels of interest. The static region should either be close to the ROI to be analyzed, or the spatial dependence of the errors should be accommodated. For the analysis shown in Fig. 7, a constant plus linear fit to the apparent velocities in the chest wall was used to estimate the velocity offsets.

The SNR in measured flow is maximized when strong flow-encoding (small v_{enc}) is used (Eq. 6). However, flow aliasing can corrupt the measurement, so either v_{enc} must be large enough to prevent aliasing or aliasing corrections should be used.

SAMPLE APPLICATIONS

The potential benefits of MRI for the evaluation of cardiovascular structures has been well established (1,4–6). The enhancements brought by phase contrast cine MRI include the ability to evaluate the presence, direction, and temporal dynamics of flow both qualitatively and quantitatively. The velocity-dependent contrast, with the intrinsic suppression of static structures, adds improved sensitivity to slow flow and its differentiation from thrombus. As a result, phase contrast cine offers enhanced char-

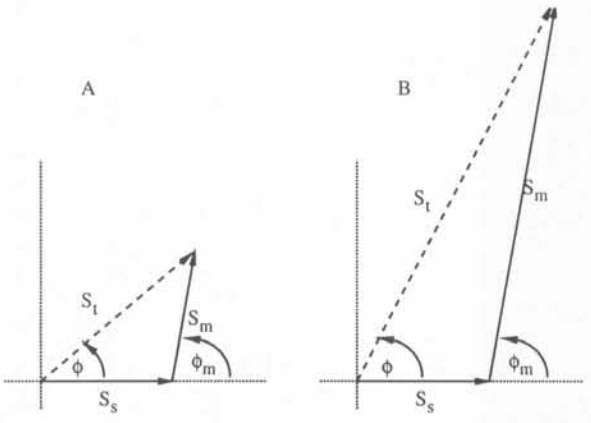

FIG. 8. A: The total signal in a voxel is the vector sum of the signal from static spins S_s and the signal from moving spins S_m. The apparent phase shift is intermediate between the motion-induced phase shift Φ_m and zero. If the relative signal from moving spins reflects the volume fraction occupied by them, the partial volume error on flow measurements is small. B: Spin replacement causes the signal from moving spins to be enhanced, the total signal to be dominated by signal from moving spins, and the flow through the voxel to be overestimated.

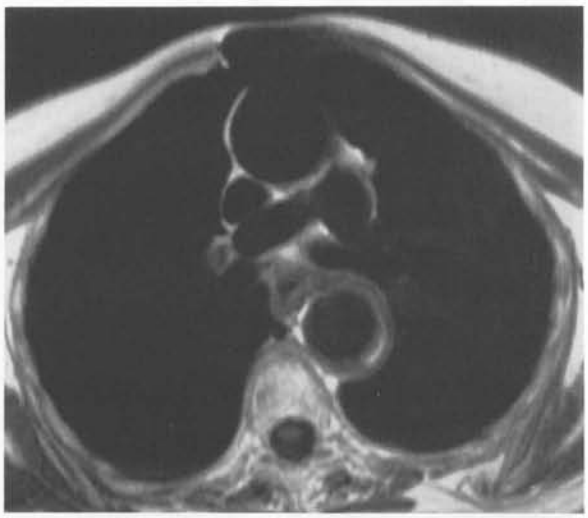

FIG. 9. ECG gated spin-echo image (TR/TE = 978/15 ms) through the mediastinum of a patient postsurgery for the repair of a type A aortic dissection. Note the crescentic area of intermediate signal with an additional crescentic area of increased signal in the posterior descending aorta. The possibility of a residual false lumen or intermural thrombus was addressed.

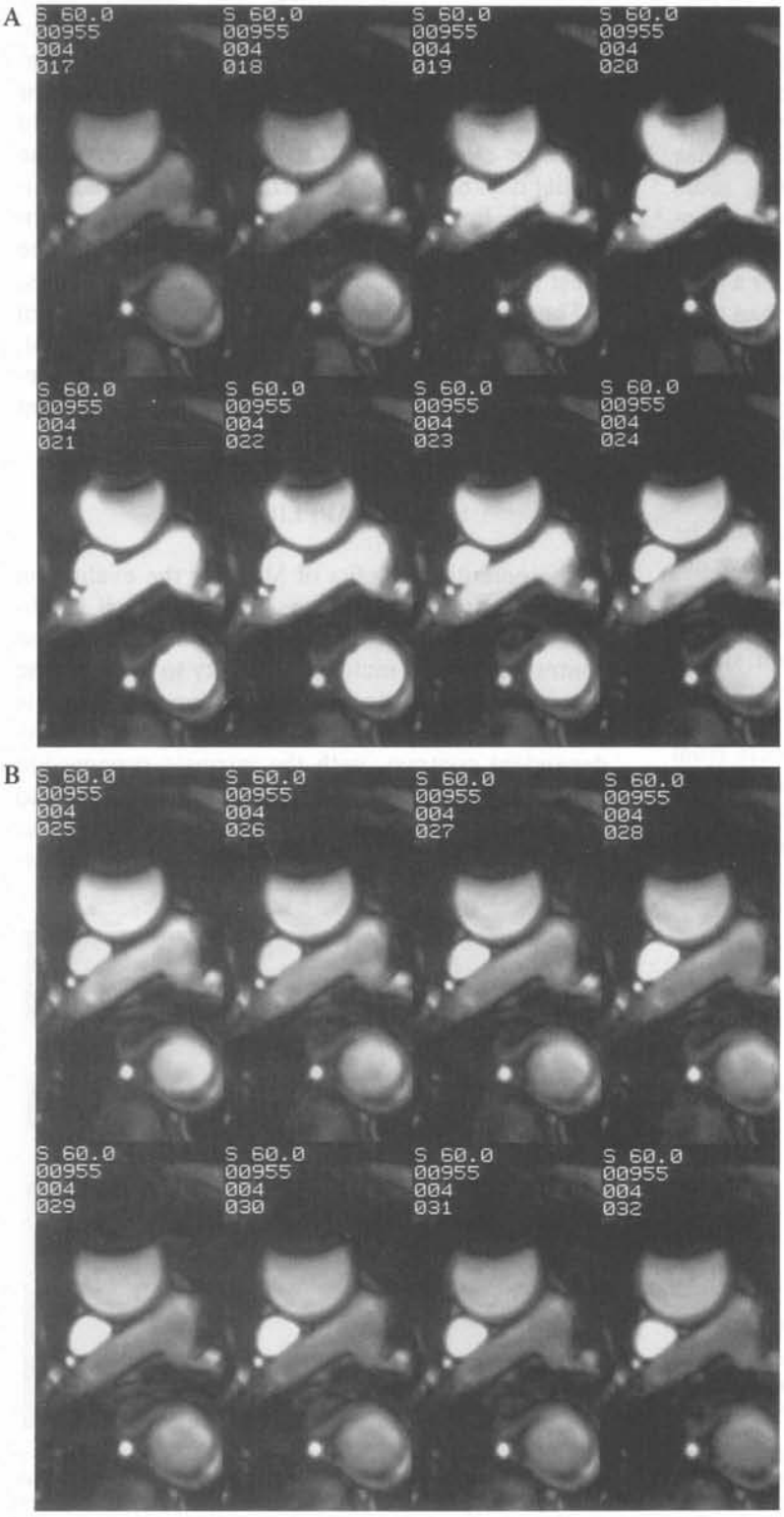

FIG. 10. Magnitude images for the first (A) and second (B) halves of the cardiac cycle for the same patient and level as in Fig. 9. Note the crescentic area of increased signal intensity corresponding to the questionable area in Fig. 9. The loss of signal intensity in the anterior portion of the ascending aorta is secondary to the patient's sternal wires.

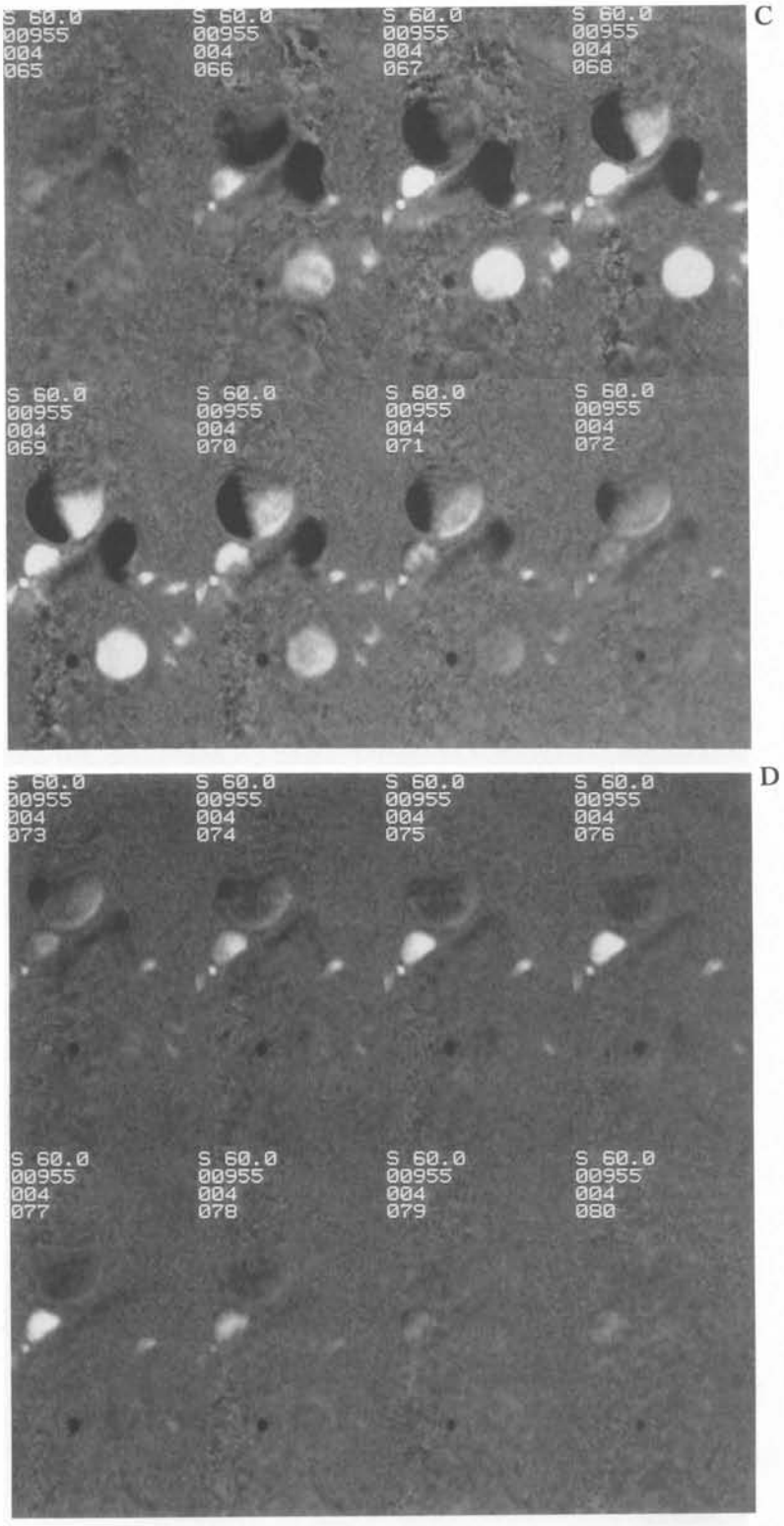

FIG. 10. C and D: Flow images encoded for motion in the cranio-caudal direction corresponding to A and B, respectively. Cranial flow is displayed as dark, whereas caudal flow is bright. No flow is seen in the area in question.

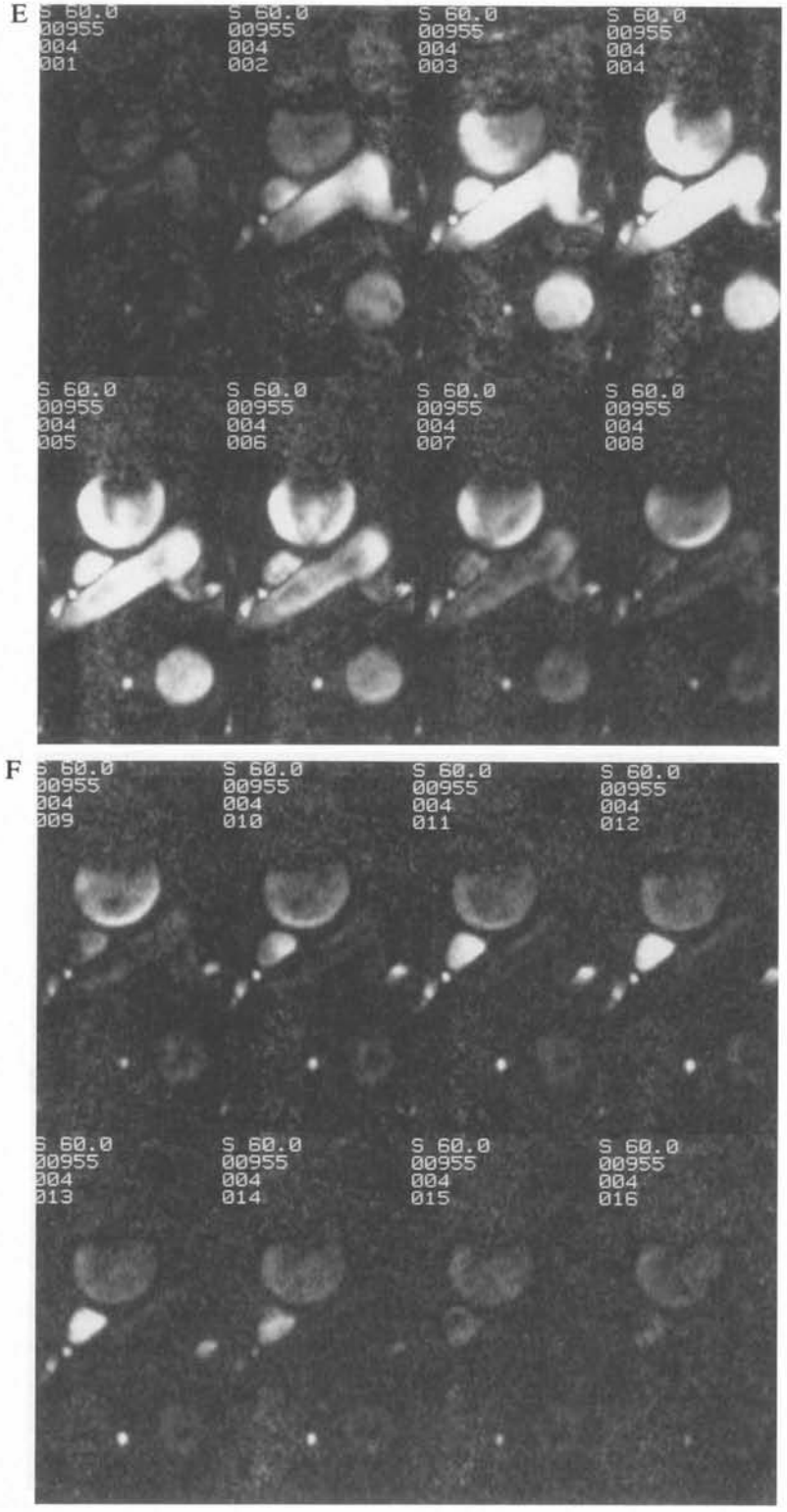

FIG. 10. **E and F:** "Speed" images in which flow is displayed as bright regardless of direction. Note the excellent suppression of static structures and absence of flow signal in the questioned crescentic area.

acterization of pathologic and normal structures, thus improving the specificity and sensitivity of routine MRI.

Figure 9 shows a spin-echo image in a patient who underwent surgery for a type A dissection. There is significant thickening of the descending aorta with relative high signal intensity located posteriorly in the midst of a crescentic area of intermediate signal intensity. The possible extension of the dissection into the descending aorta was suggested. Figure 10A and B shows the magnitude images for 16 frames of the cardiac cycle at the same level from a phase contrast cine acquisition encoded for flow in all directions (Fig. 3B). These magnitude images show the crescentic area identified on the spin-echo image as a region of decreased signal, with an area

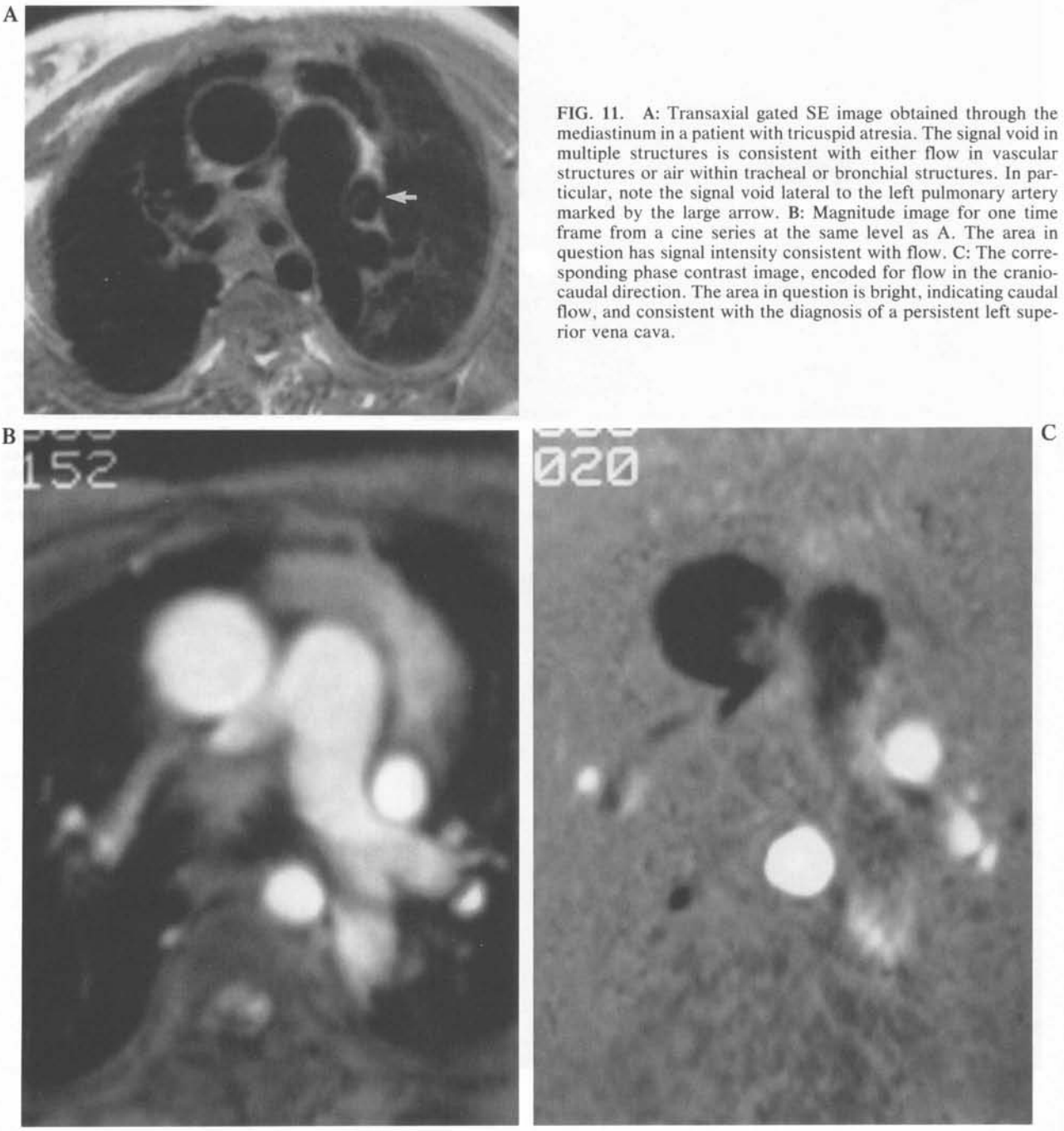

FIG. 11. A: Transaxial gated SE image obtained through the mediastinum in a patient with tricuspid atresia. The signal void in multiple structures is consistent with either flow in vascular structures or air within tracheal or bronchial structures. In particular, note the signal void lateral to the left pulmonary artery marked by the large arrow. B: Magnitude image for one time frame from a cine series at the same level as A. The area in question has signal intensity consistent with flow. C: The corresponding phase contrast image, encoded for flow in the craniocaudal direction. The area in question is bright, indicating caudal flow, and consistent with the diagnosis of a persistent left superior vena cava.

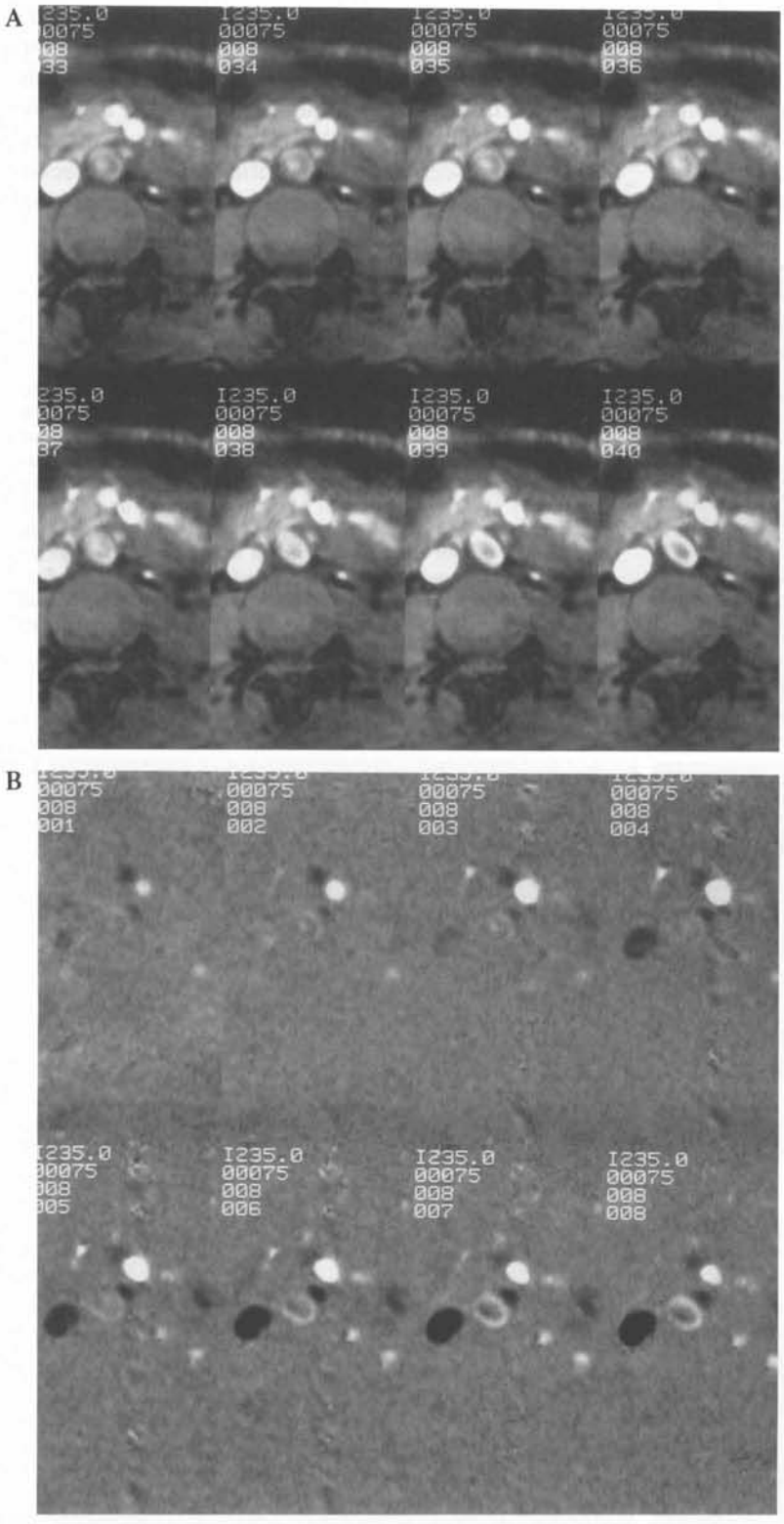

FIG. 12. A: Magnitude images for the first eight of 16 frames in the cycle through the midabdominal aorta from a phase contrast cine study of a patient with an abdominal aortic coarctation. B: The corresponding flow images, encoded in the superior–inferior direction. Note the complex flow within the abdominal aorta. The relatively large collateral arterial pathways are recognized by bright appearance in B, indicating superior-to-inferior flow.

of slight increase in signal suggesting a potential false lumen in the descending aorta. Figure 10C and D shows the corresponding images encoded for flow in the superior–inferior direction. Complex flow in the somewhat large ascending aorta can be identified as areas of mixed directional flow (28). The bright appearance of the descending aorta indicates consistent caudal flow, and there is no significant flow signal in the crescentic area to suggest either superior or inferior flow in the false lumen of a dissection. Figure 10E and F shows the speed images obtained by combining information from all the flow directions, and in which bright appearance represents flow without regard to direction. With excellent suppression of background structures, no flow can be seen in the crescentic area of the descending aorta, suggesting that the bright signal noted on both the magnitude images and the spin-echo images most likely represents clot or methemoglobin formation in the wall of the descending aorta (29).

The directional information provided by phase contrast cine MRI aids in the identification of individual anatomic structures. Figure 11A shows a spin-echo image through the mediastinum in a patient with tricuspid atresia, with vascular structures displaying typical signal voids. In complex congenital heart disease, however, the separation of bronchi, arteries, and veins can sometimes be perplexing. For example, note the large signal void lateral to the left main pulmonary artery. Figure 11B shows the magnitude images from a phase contrast cine acquisition. Early in the cardiac cycle, the area of signal void seen on the spin-echo image is bright and indicates flow in a vascular structure. On the flow images encoded for flow in the superior–inferior direction (Fig. 11C), this area is bright consistent with caudal flow. Additionally, there is absence of marked caudal flow on the right side, the normal location of the superior vena cava. This finding is characteristic of a persistent left superior vena cava. Note how easily the presence and direction of flow of the vasculature within the pulmonary hila can be identified. This may greatly enhance the ability to size and localize pulmonary arteries in patients with relative pulmonary atresia, and may help identify the origin of flow in collateral bronchial vasculature (30). The relatively high contrast of vascular structures emphasizes cranial flow in the azygous vein, seen posteriorly on the right in this particular patient. This type of directional flow information may be extremely useful in identifying collateral vasculature, as well as reversal of flow in the presence of steal syndromes, and can aid in the definition and characterization of complex vascular structures in congenital heart disease.

The ability to characterize direction, pulsatility, and complexity of flow not only improves the diagnostic accuracy but may provide unique insights into pathologic processes. Phase contrast cine MRI is particularly useful in areas not easily accessible by Doppler or where the complex flow of a pathologic process may provide confusing data. Figure 12A and B shows magnitude and flow images, respectively, for the first eight frames of a 16-frame phase contrast study obtained transaxially in the abdomen of a patient with an abdominal corarctation and encoded for flow in the superior–inferior direction. Many collateral arterial pathways can be identified as bright structures in Fig. 12B. An enlarged superior mesenteric artery can be identified just anterior to the aorta and several smaller vessels can be detected in the retroperitoneum. The aorta itself shows a complex flow pattern. The superiorly directed (dark) flow in the central portion represents retrograde filling just inferior to the total occlusion of the abdominal aorta, which then reverses direction and flows caudally at the periphery. The excellent suppression of static structures and the detailed flow information provided by phase contrast cine may provide important information for surgical therapy in a number of complex lesions.

Interleaved acquisition of flow information in all

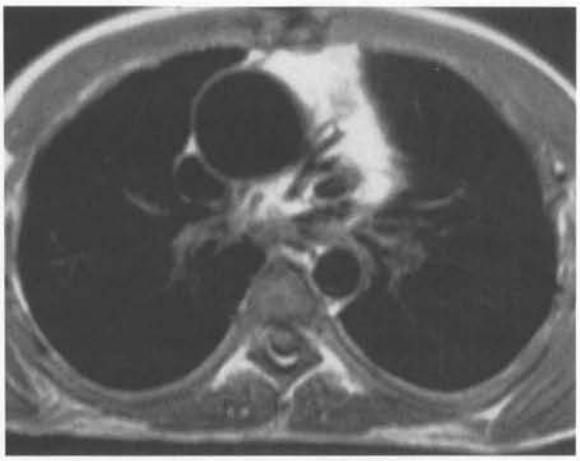

FIG. 13. ECG-gated SE image obtained transaxially in the mediastinum of a patient with complex congenital heart disease including pulmonary atresia. Of great clinical interest in this case was the presence or absence of appropriate pulmonary vascularity for potential surgical correction. Note the large number of signal voids in the mediastinum and hilar regions (see Fig. 14).

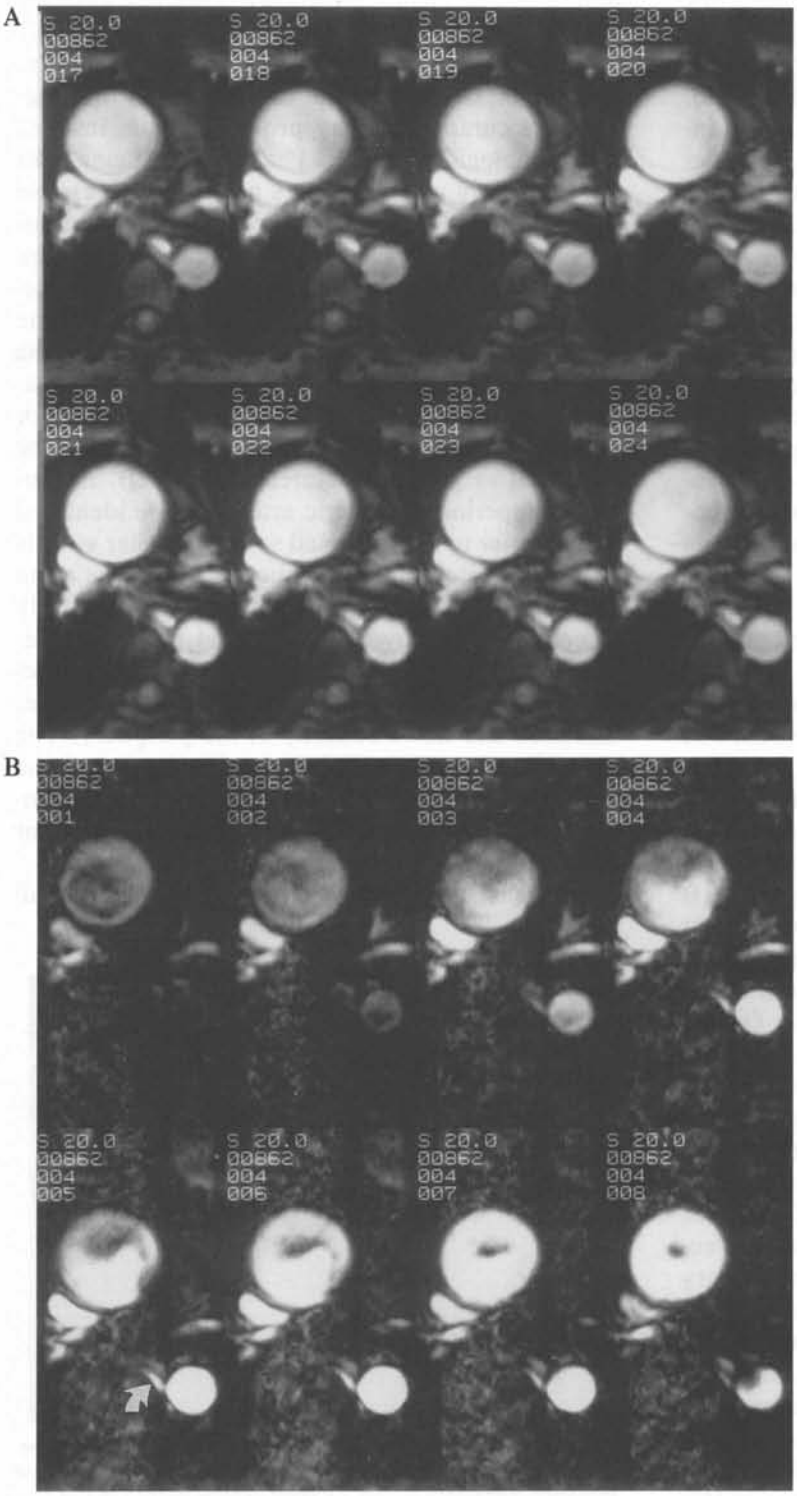

FIG. 14. Images for the first eight of 16 frames in the cycle from a phase contrast cine acquisition at the same level as Fig. 13 and encoded for flow in all directions **A and B**: Magnitude and speed images, respectively.

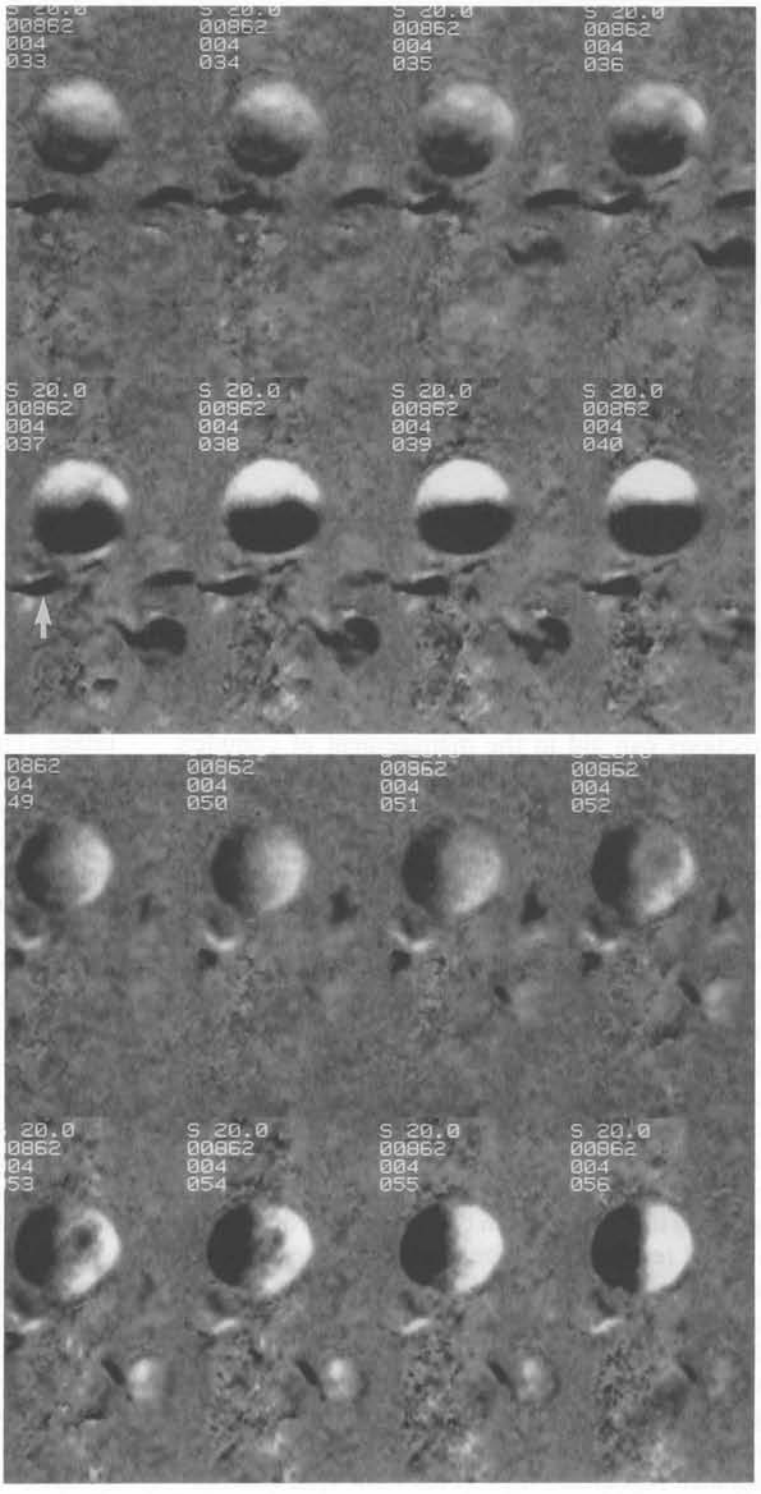

FIG. 14. C–E: The corresponding direction-sensitive images, displaying the right–left, anterior–posterior, and superior–inferior flow components, respectively. Note on the speed images (B) an area of prominent velocity adjacent to the abdominal aorta representing a large main pulmonary collateral artery. Additionally, on the right–left images (C) there is a prominent dark region (flowing left to right, toward the right lung) in the right hilum and mediastinum consistent with a moderate sized (6 mm) right pulmonary artery.

E

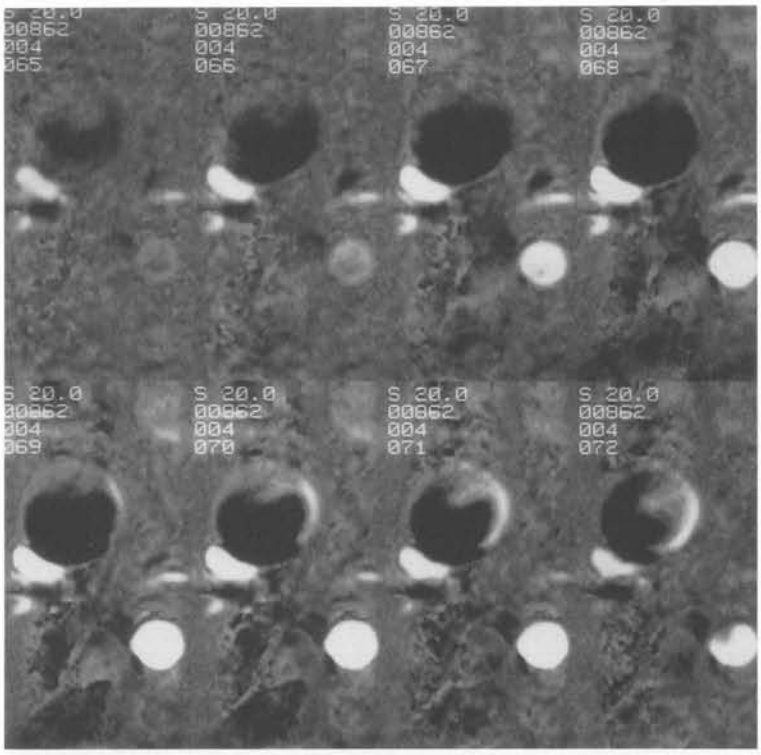

FIG. 14. E. See legend on preceding page.

directions can aid in the management of complex congenital heart disease. Figure 13 shows the spin-echo image of a patient with pulmonary artery atresia who was being evaluated for possible corrective surgery. A number of low signal areas are seen in the mediastinum and hila, which may represent pulmonary vascular structures and could provide sources for potential surgical correction. Cine MRI can separate vascular from bronchial structures, as demonstrated in Fig. 14A which shows magnitude images for the first eight of 16 frames of a phase contrast acquisition encoded for flow in all directions (equivalent to conventional cine MRI). However, this still leaves a relatively complex picture. Figure 14B shows the corresponding speed images in which brightness is proportional to speed regardless of direction. Note the excellent background suppression and the ability to identify high-flow structures by their relatively high image intensity. Also of note is the complex behavior of the signal intensity within the ascending aorta. Images sensitive to flow in individual directions are presented in Fig. 14C–E. In Fig. 14C–E, bright appearance represents flow in the right–left, anterior–posterior, and superior–inferior directions, respectively. These images provide improved characterization of the pathologic state. On the right–left image (Fig. 14C) in the right hilum, the relatively dark (flowing into the lung) prominent vessel measuring ~6 mm is the right main pulmonary artery. The vessel flowing from left to right (dark) from the descending aorta and anterior to the spine is a large main pulmonary collateral artery. Of equal importance is the absence of significant flow from right to left in the left hilum. The complex flow in the ascending aorta can be appreciated by comparing the right–left and anterior–posterior data (Fig. 14C and D). This segmented black/white appearance is consistent with spiraling of blood up the ascending aorta. The cranial component is seen on the superior–inferior images (Fig. 14E). Although some spiraling flow in the ascending aorta is expected, this pattern appears to be emphasized in this patient with complex congenital heart disease. These insights into patterns of flow within vessels may provide additional information and help characterize various pathophysiologic states (31–33).

Figure 15 shows images obtained transaxially on a patient with a type B aortic dissection. Magnitude images (Fig. 15A and B) clearly demonstrate the presence of an intimal flap in the descending aorta. On the flow images (Fig. 15C and D), encoded for flow in the superior–inferior direction, the true lumen of the dissection can be identified as having

consistent superior-to-inferior flow whereas the false lumen has a more disordered appearance and blunted velocities. The temporal characteristics are graphically demonstrated in Fig. 16. Recent work (29) has shown that phase contrast cine MRI, when combined with routine spin-echo imaging, significantly enhances the confidence level of diagnoses for the presence or absence of aortic dissections. The ability to clearly identify areas of flow as well as the pulsatile natue of velocity adds significant diagnostic information.

The ability to quantitate flow is a potentially powerful aspect of phase contrast cine MRI. The method does not need an appropriate acoustic window, provides excellent temporal data throughout the cardiac cycle, and easily evaluates the edges of vessels. The quantitative nature of this technique has been explored in a number of areas. Flow rate waveforms and average flow rates in the cerebral circulation of normals (34) and patients with arteriovenous malformation (35) have been measured. The ability to directly measure flow within the aorta has been suggested as a method for evaluating aortic compliance and coronary artery blood flow. Caudal flow in the ascending aorta in patients with normal aortic valve function, as seen in Figs. 7 and 16, may represent flow toward the coronary circulation. In the presence of aortic insufficiency it can be used directly to quantitate valvular regurgitant volumes. Caputo et al. have suggested that quantitative pulmonary flow measurements may be useful in evaluation of patients with acquired and congenital lesions affecting pulmonary blood flow (36). Cardiac output can easily be calculated by measuring the forward flow through the aorta. Cardiac shunts can be evaluated by comparing left-sided cardiac output as measured at the aorta with the right sided output as measured at the pulmonary artery (37). Figure 17 is a graph comparing the flow rate throughout the cycle and cardiac output from the right and left ventricles in a patient with a ventricular septal defect and Eisenmenger syndrome. The ratio of right-to-left output (QP/QS) in this case was 0.72.

Phase contrast cine MRI has utility outside the cardiovascular system, such as the "third circulation," i.e., cerebrospinal fluid (CSF) flow. Whereas the presence of cardiosynchronous brain motion and CSF flow have been known for many decades, little is known about the detailed patterns of this motion and their disruption in pathological conditions. Measuring flow in this system is difficult because CSF is not confined to vascular structures. Phase contrast cine has provided a major advance in investigation of CSF flow.

CSF flow dynamics in normal volunteers have been studied with phase contrast cine (38), and some data has been accumulated about CSF flow in syringomyelia. Figure 18 shows the results from a 16-frame phase contrast cine study of a 56-year-old woman with syringomyelia secondary to a Chiari I malformation. The low position of the cerebellar tonsils, visible on the magnitude images (Fig. 18A), causes obstruction of CSF flow at the level of the foramen magnum and is felt to be a factor in the pathogenesis of cyst formation in the spinal cord. Figure 18B and C shows the flow images, encoded for motion in the cranio-caudal direction with v_{enc} = 15 cm/s, and synchronized to the cardiac cycle using an ECG trigger. These sagittal images show the temporal relationships of the oscillatory motion of the CSF, spinal cord, and lower brainstem. In frame 3, the cervical cord, lower brainstem, and cerebellum move in the caudal direction (bright) while the CSF is still moving in cranially (dark). In the next frame (frame 4), CSF flow in the cervical subarachnoid space (SAS) has reversed and is in the caudal direction (white). Whereas onset of systolic cranio-caudal flow in the syrinx is simultaneous with SAS flow (frame 4), flow in the syrinx cavity ceases and reverses before that in the cervical SAS (frame 8 vs. frame 11). This pattern, nearly simultaneous onset of cranio-caudal flow in the syrinx and SAS but earlier flow reversal in the syrinx, is typical of syringomyelia and may be due to the syrinx being a shorter closed-end structure than the SAS.

Treatment of syringomyelia consists of a suboccipital decompression with removal of bone and release of the tonsils. This opens CSF flow pathways at the level of the foramen magnum, and results in cessation of flow and a slow decrease in size and eventual collapse of the syrinx. Much remains to be learned about CSF flow dynamics. Further experience may allow phase contrast cine to be used in earlier identification of surgical candidates, in surgical follow-up, and in the evaluation of new therapies. Phase contrast cine is also being used in efforts to understand normal pressure hydrocephalus.

FUTURE DIRECTIONS

The expected advances in phase contrast cine can be divided into two general areas: further technical

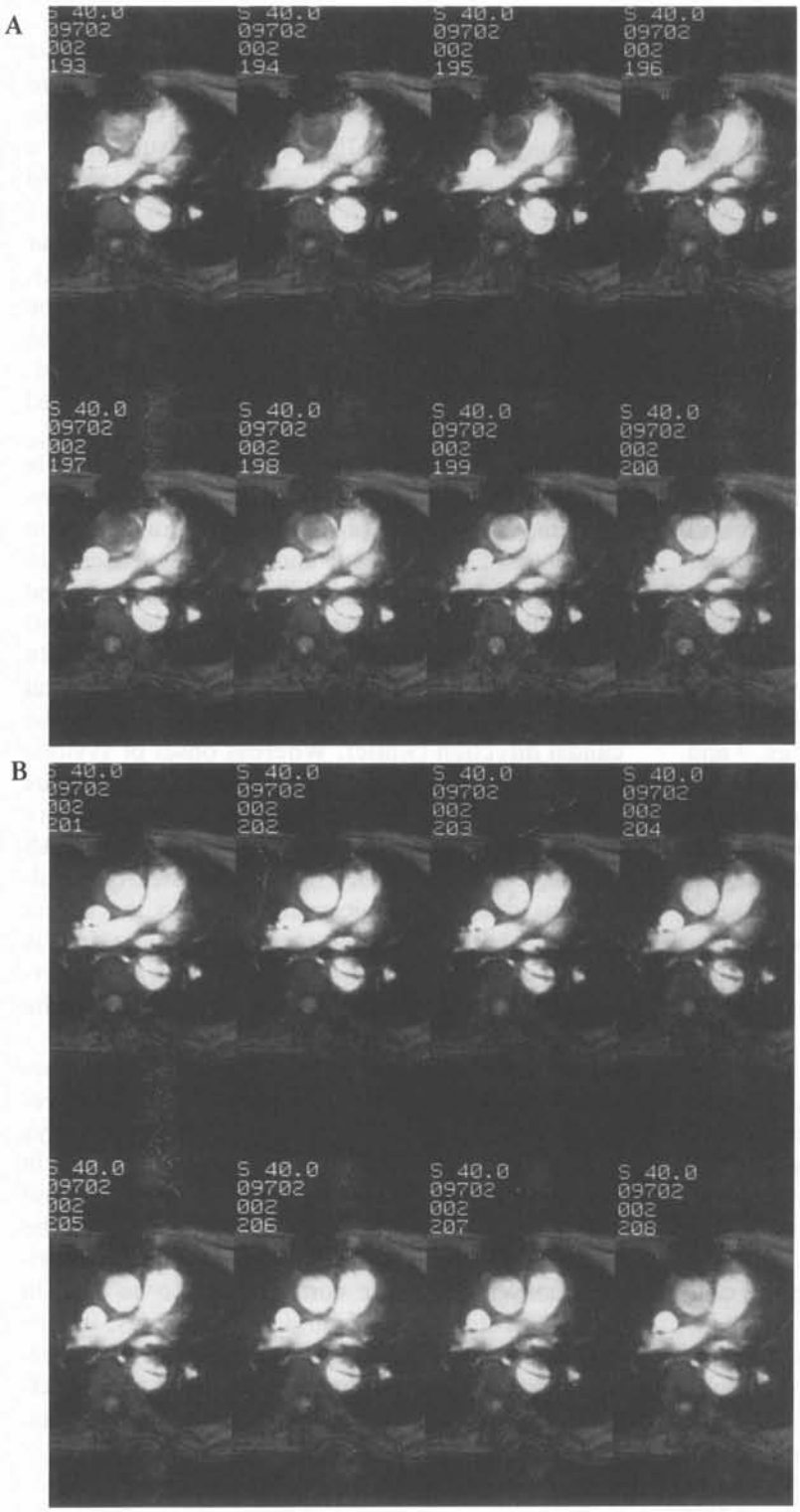

FIG. 15. **A and B:** Magnitude images for the first and second halves of the cycle, respectively, obtained in a patient with an aortic dissection.

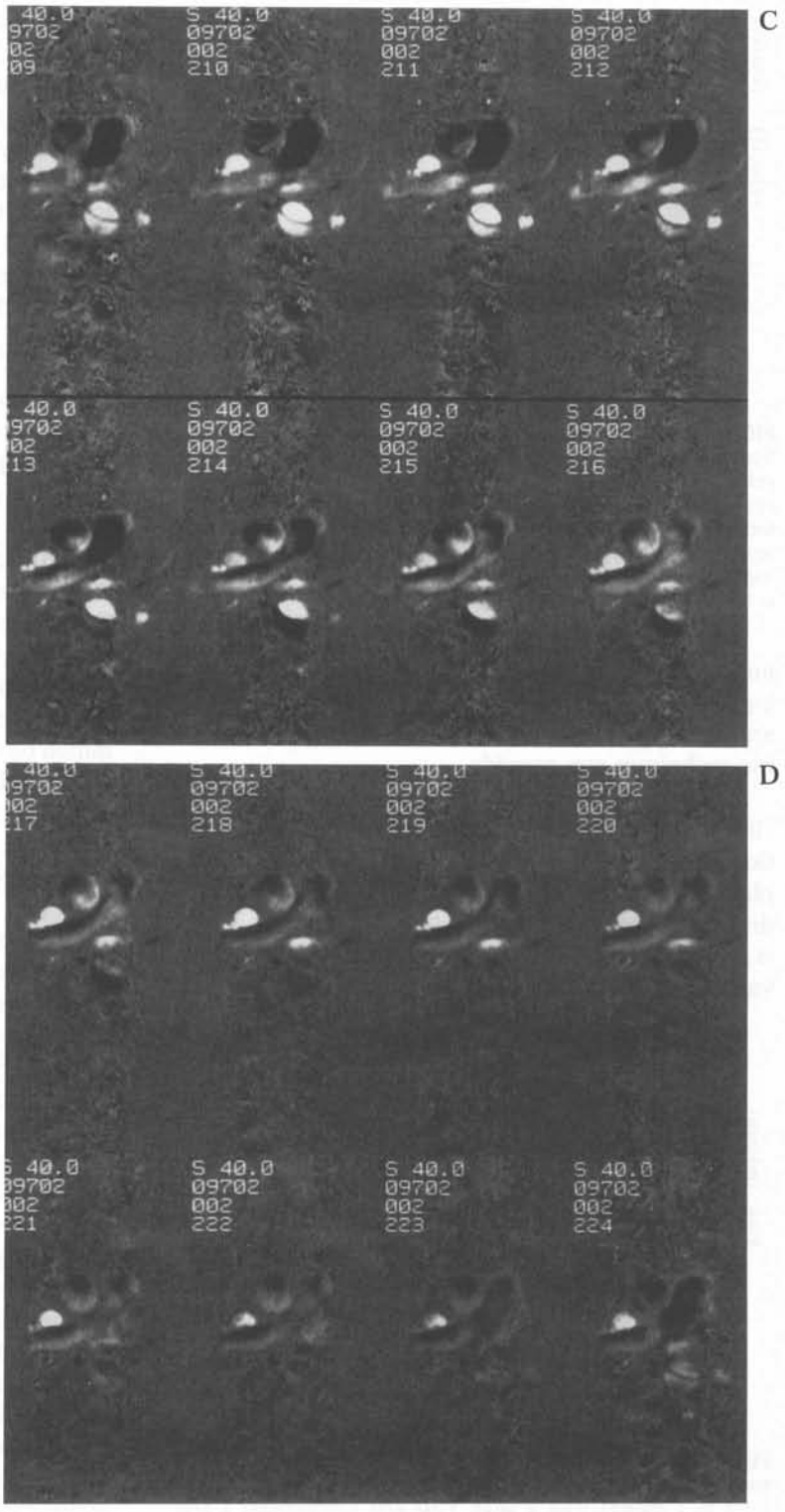

FIG. 15. C and D: The corresponding superior–inferior encoded phase contrast cine MRI images. There is strong caudal flow (bright) in both lumens of the descending aorta in the beginning of the cycle, with prominent reversal of flow (bright to dark) in the false lumen late in the cycle.

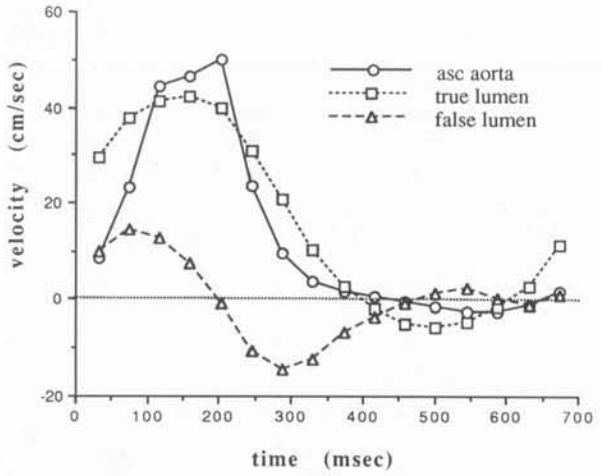

FIG. 16. Plot of flow velocity during the cardiac cycle derived from the data in Fig. 15. Note the reversal of flow (negative velocities) in the false lumen in the midportion of the cardiac cycle. Note also the caudal flow (negative velocity) seen in the ascending aorta in diastole. It has been suggested that this may represent coronary flow and may provide a method for measuring total coronary flow. However, this finding would also occur in the presence of aortic insufficiency.

improvements including shorter acquisition times, higher temporal resolution and enhanced accuracy, and new applications of the quantitative data that the technique can provide.

Present implementations examine one or two slices with an imaging time of a few minutes. Additional coverage is provided by concatenating multiple acquisitions. The acquisition of data over hundreds of cardiac cycles has two drawbacks. There is, no doubt, degradation in the data resulting from variability of the cardiac cycle, especially in patients with arrhythmia. Also, the present acquisition time precludes imaging during suspended respiration, and, even when respiratory compensation is used, respiratory motion leads to motion artifacts and resolution loss. These limitations may be overcome by the incorporation of phase contrast into the newly developed ultrafast imaging techniques such as echo-planar imaging (39), spiral k-space scanning (40), or segmented k-space methods with ultrashort TR (41), although the impact on SNR and spatial resolution must be studied.

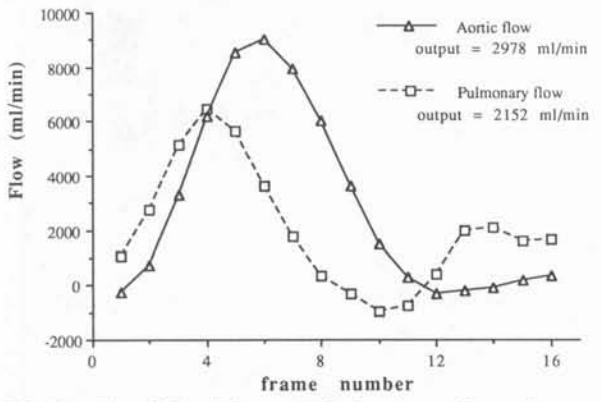

FIG. 17. Plot of blood flow rate during the cardiac cycle measured with phase contrast cine in the main pulmonary artery and aorta of a patient with a large VSD and Eisenmenger's syndrome. These data are consistent with a right-to-left shunt, which would be difficult to evaluate precisely with conventional methods.

When the various sequence types are rapidly interleaved, the temporal resolution of the current technique is on the order of 40–100 ms. Although this is satisfactory for many applications, it may be inadequate for some, such as studies involving patients with rapid heart rates. In addition, improved temporal resolution may improve image quality by reducing inconsistencies in temporal registration within each image. TR shortening offers the most direct method for improving temporal resolution. Other approaches include discarding the interleaving of sequence types and/or using interleaved temporal sampling over multiple heart cycles.

The precision of the phase contrast data is determined by the flow encoding strength, the underlying NMR SNR, and the presence of other stochastic errors such as flow or motion-related artifacts. The latter effects have been discussed. Use of optimized surface coils and/or coil arrays will increase the SNR and therefore improve the quality of the data. Also, as automated phase unwrapping methods are developed and adopted, stronger flow encoding may be used for improved precision with decreased fear of velocity aliasing.

The superb suppression of static structures on the speed images coupled with the temporal resolution of this cine technique may provide a method for enhanced qualitative assessment of cardiovascular structures in projection format. Figure 19 shows anteroposterior angiograms at multiple frames in the cardiac cycle generated from four contiguous coronal phase contrast cine data sets encoded for flow in all directions. For each frame in the cardiac cycle, the speed images at each slice were collapsed by maximum intensity projection (MIP). This patient had surgical repair for transposition of the great vessels with resultant occlusion of the superior vena cava. Patency of the graft from the left internal jugular vein to the right atrium is demonstrated.

The quantitative utilization of phase contrast cine data may produce a wide range of new clinical ap-

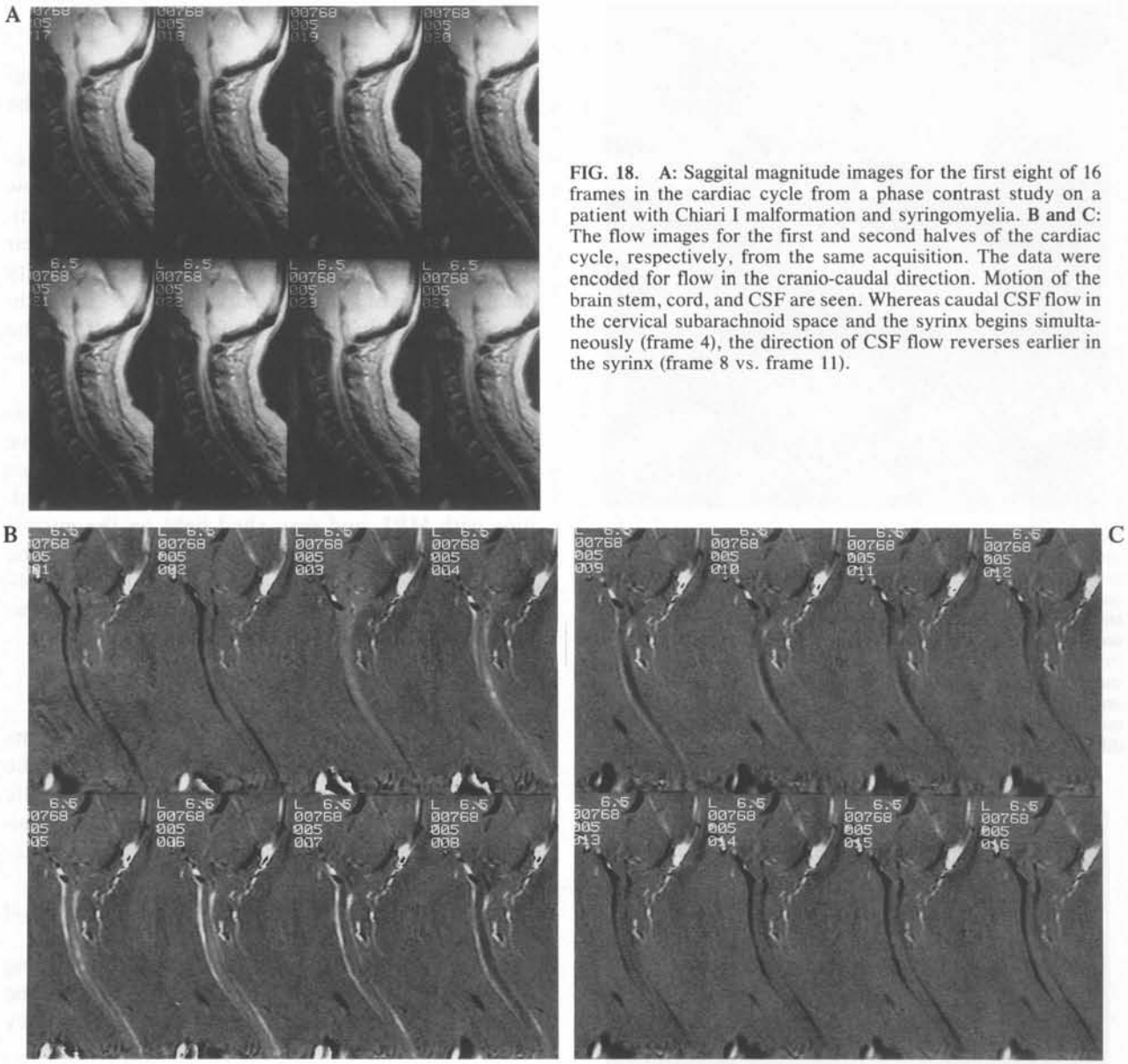

FIG. 18. A: Saggital magnitude images for the first eight of 16 frames in the cardiac cycle from a phase contrast study on a patient with Chiari I malformation and syringomyelia. **B and C:** The flow images for the first and second halves of the cardiac cycle, respectively, from the same acquisition. The data were encoded for flow in the cranio-caudal direction. Motion of the brain stem, cord, and CSF are seen. Whereas caudal CSF flow in the cervical subarachnoid space and the syrinx begins simultaneously (frame 4), the direction of CSF flow reverses earlier in the syrinx (frame 8 vs. frame 11).

plications. Whereas some validation of the quantitative accuracy of this technique has been performed (37,42), additional validation, particularly in vivo and in situations that are relevant to the envisioned applications, is needed. Improved utility can be expected with improved correction for eddy current–induced phase shifts and with automated ROI definition methods that can track vessels throughout the cycle.

Quantitative applications of phase contrast data that extend beyond measurement of velocity and flow rate are being developed. With sufficiently strong motion encoding, phase contrast techniques can measure motion velocity within the myocardium (14). Velocity maps at multiple frames throughout the cardiac cycle can then be used to study the motion of the myocardium, much as is done with spin tagging methods (43,44). The motion of a selected region, defined at the first time frame, is computed using the velocity data and an algorithm that recursively estimates the location of the region in each frame (45). This can be repeated for any number of regions. Figure 20 shows four of sixteen frames in the cycle, and the computed locations of selected regions are shown as bright squares. Four regions have been connected with

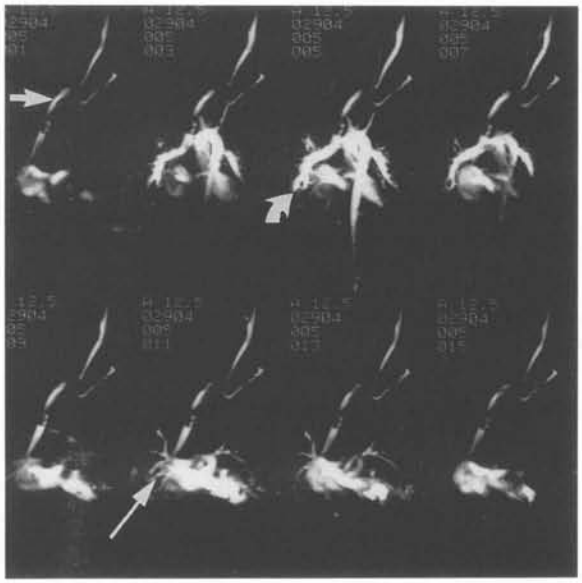

FIG. 19. Time-resolved anteroposterior MR angiographic images for every other frame in the cardiac cycle on a patient who underwent surgical repair for transposition of the great vessels and occlusion of the superior vena cava. Phase contrast cine data encoded for flow in all directions was acquired for four contiguous coronal sections. The speed images at each frame were "collapsed" using maximum intensity projection. The graft from the left internal jugular vein to the right atrium is seen (short arrow). Note that maximum contrast in the pulmonary arteries (curved arrow) and pulmonary veins (long arrow) is observed at different times in the cycle.

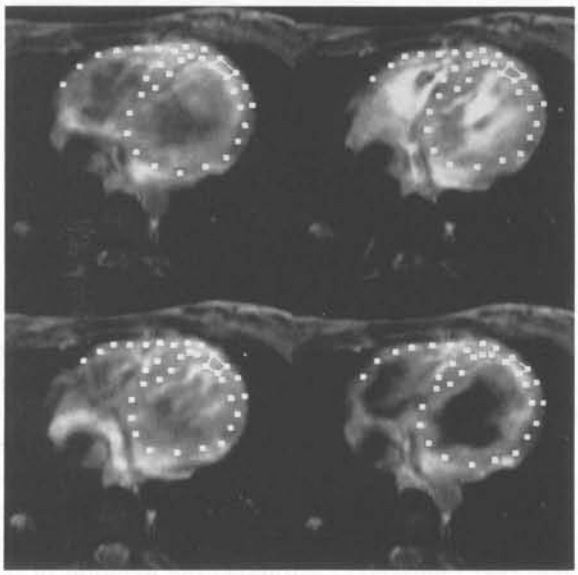

FIG. 20. Four of sixteen images throughout the cardiac cycle demonstrating the use of phase contrast cine MRI data to track myocardial motion. Phase contrast data encoded for motion in all directions was acquired in this patient with a small apical metastasis. Each bright square graphical overlay represents a small myocardial region, the position of which was defined in frame 1. The phase contrast velocity data were used to compute the motion of each region, and the resulting locations are displayed on the magnitude images from the same acquisition. Four of the regions are connected with lines to help visualize wall thickening and segmental shortening. Marked contraction of the right ventricle is evident.

lines to help visualize the wall thickening and segmental shortening that are demonstrated by the method.

In a related method, Napel et al. (46) use three-dimensional (3-D) velocity maps to calculate flow streamlines. In this technique, a set of seed particles is defined within a vessel of interest and their motion is computationally derived from the velocity data. Because of imaging time constraints, the technique is presently limited to ungated data. It may be greatly aided by the development of 3-D phase contrast cine.

Phase contrast cine MRI is an efficient and flexible technique for the qualitative and quantitative study of flow characteristics. It greatly enhances the clinical evaluation of cardiovascular abnormalities with MRI, and may shed light on the normal and pathologic physiology of CSF flow. As the technical development continues and clinical applications are validated, its role will continue to grow.

APPENDIX

The instantaneous precession frequency of spins is the product of the local magnetic field B and the gyromagnetic ratio γ. In the presence of a magnetic field gradient, the field B depends on spatial position. Considering a gradient in the x direction G_x:

$$B = B_o + G_x x \tag{A1}$$

It is simplest at this point to move to the rotating frame (rotating at frequency γB_o) to account for the effect of B_o. In this rotating frame the frequency ω is

$$\omega = \gamma G_x x. \tag{A2}$$

The frequency ω may be a function of time t due to the time dependence of the gradient $G_x(t)$, and due to the time dependence of the x position (i.e., motion), which can be expressed as

$$x(t) = x_o + vt + \frac{1}{2} at^2 + \cdots, \tag{A3}$$

where x_o, v, and a are the position, velocity, and acceleration of the spins at time $t = 0$, respectively.

The frequency ω is the rate at which signal phase ϕ_s is increasing. As a result, the phase at time T, $\phi_s(T)$, is the integral of ω from the time the trans-

verse magnetization was excited ($t = 0$) until time T:

$$\phi_s(T) = \int_0^T \omega(t)\, dt. \qquad \text{(A4)}$$

Combining Eqs. A2, A3, and A4, we have

$$\phi_s(T) = x_o \left\{\gamma \int_0^T G_x(t)\, dt\right\} + v \left\{\gamma \int_0^T G_x(t)\, t\, dt\right\} + a \left\{\frac{1}{2}\gamma \int_0^T G_x(t)\, t^2\, dt\right\} + \cdots, \qquad \text{(A5)}$$

where we have ignored the effects on phase of processes other than motion through gradients (e.g., local magnetic field inhomogeneities). The signal phase has contributions from position x_o, velocity v, and, in general, higher order terms. The first term in Eq. A5 is proportional to position x_o and to the area under the gradient waveform, and can be referred to as position encoding. The second term is proportional to velocity and can be referred to as the velocity-encoding term, and so on. The position-encoding term is responsible for MR's ability to produce spatially localized images and is taken into account in the Fourier transform used to produce images. To a good approximation, the phase in a reconstructed image ϕ is

$$\phi = v \left\{\gamma \int_0^{TE} G_x(t)\, t\, dt\right\} + a \left\{\frac{1}{2}\gamma \int_0^{TE} G_x(t)\, t^2\, dt\right\} + \cdots, \qquad \text{(A6)}$$

where TE is the echo delay time (i.e., the time at which the center of k-space was measured). Whereas position encoding is proportional to the area under the gradient (zeroeth moment, see Eq. A5), the velocity term is proportional to the first moment, M_1, of the gradient waveform, where

$$M_1 = \int_0^{TE} G_x(t)\, t\, dt. \qquad \text{(A7)}$$

Similarly, the acceleration term is proportional to the second moment of the gradient, M_2:

$$M_2 = \int_0^{TE} G_x(t)\, t^2\, dt. \qquad \text{(A8)}$$

For most phase contrast MRI, the acceleration and higher terms are ignored.

Acknowledgement: Countless discussions with Gary H. Glover were very enlightening, as always, during the evolution of this work. We thank Donna Cronister for technical assistance during the preparation of this manuscript.

REFERENCES

1. Peshock R. Clinical cardiovascular magnetic resonance imaging. *Am J Cardiol* 1990;66:41F–4F.
2. Glover GH, Pelc NJ. A rapid-gated cine MRI technique. In: Kressel HY, ed. *Magnetic resonance annual 1988*. New York: Raven, 1988:299–333.
3. Utz JA, Herfkens RJ, Heinsimer JA, et al. Cine MR determination of left ventricular ejection fraction. *AJR* 1987;148: 839–43.
4. Sechtem U, Pflugfelder PW, Gould RC, Cassidy MM, Higgins CB. Measurement of right and left ventricular volumes in healthy individuals with cine MR imaging. *Radiology* 1987;163:697.
5. Sechtem U, Pflugfelder PW, Cassidy MM. Cine MR determination of left ventricular ejection fraction. *Radiology* 1988;167:425.
6. Higgins C, Holt W, Pflugfelder P, Sechtem U. Functional evaluation of the heart with magnetic resonance imaging. *Magn Reson Med* 1988;6:121.
7. Nayler GL, Firmin DN, Longmore DB. Blood flow imaging by cine magnetic resonance. *J Comput Assist Tomogr* 1986; 10:715–22.
8. Hahn EL. Detection of sea-water motion by nuclear precession. *J Geophys Res* 1960;65:776–7.
9. Grover T, Singer JR. NMR spin-echo flow measurements. *J Appl Physiol* 1971;42:938.
10. Moran PR. A flow velocity zeugmatographic interlace for NMR imaging in humans. *Magn Reson Imaging* 1982;1:197–209.
11. Feinberg DA, Crooks LE, Sheldon P, Hoenninger J, Watts J, Arakawa M. Magnetic resonance imaging the velocity vector components of fluid flow. *Magn Reson Med* 1985;2: 555–66.
12. Hennig J, Muri M, Brunner P, Friedburg H. Quantitative flow measurement with the fast Fourier flow technique. *Radiology* 1988;166:237–40.
13. Dumoulin CL, Souza SP, Hardy CJ, Ash SA. Quantitative measurement of blood flow using cylindrically localized Fourier velocity encoding. *Magn Reson Med* 1991;21:242.
14. Van Dijk P. Direct cardiac NMR imaging of heart wall and blood flow velocity. *J Comput Assist Tomogr* 1984;8:429–36.
15. Bryant DJ, Payne JA, Firmin DN, Longmore DB. Measurement of flow with NMR imaging using a gradient pulse and phase difference technique. *J Comput Assist Tomogr* 1984; 8:588–93.
16. O'Donnell M. NMR blood flow imaging using multiecho, phase contrast sequences. *Med Phys* 1985;12:59–64.
17. Pelc NJ, Spritzer CE, Lee JN. A rapid flow imaging method. *Radiology* 1988;169:343.
18. Spritzer CE, Pelc NJ, Lee JN, Evans A, Sostman HD, Riederer SJ. Rapid MR imaging of blood flow with a phase-sensitive, limited-flip-angle, gradient recalled pulse sequence: preliminary experience. *Radiology* 1990;176:255–62.
19. Pelc NJ, Bernstein MA, Shimakawa A, Glover GH. Encoding strategies for three-direction phase-contrast MR imaging of flow. *J Magn Reson Imaging* 1991;1:405–13.
20. Hausmann R, Lewin JS, Laub G. Phase-contrast MR angiography with reduced acquisition time: new concepts in sequence design. *J Magn Reson Imaging* 1991;1:415–22.
21. Axel L, Morton D. Correction of phase wrapping in magnetic resonance imaging. *Med Phys* 1989;16:284–7.

22. Spraggins TA. Wireless retrospective gating: application to cine cardiac imaging. *Magn Reson Imaging* 1990;8:675–81.
23. Pelc NJ, Shimakawa A, Glover GH. Phase contrast cine MRI. *Proc Soc Magn Reson Med* 1989:101.
24. Tarnawski M, Porter DA, Graves MJ, Taylor MG, Smith MA. Flow determination in small diameter vessels by magnetic resonance imaging. *Proc Soc Magn Reson Med* 1989:896.
25. Wolf RL, Ehmann RL. Determinants of accuracy and precision in MR flow volumetry. *Proc Soc Magn Reson Med* 1991:1157.
26. Rubin DL, Herfkens RJ, Pelc NJ, Jeffrey RB. MR measurement of portal blood flow in chronic liver disease: application to predicting clinical outcome. *Proc Soc Magn Reson Med* 1990:90.
27. Higgins CB. Cine MRI: Quantitative functional evaluation of the heart. *Proc Soc Magn Reson Med* 1989:3.
28. Bogren H, Underwood S, Firmin D. Magnetic resonance velocity mapping in arterial dissection. *Br J Radiol* 1988;61: 726.
29. Herfkens R, Jeffrey R, Trefelner E, Pelc N, Lucas D. Aortic dissection: velocity encoded pulse sequence improves diagnostic accuracy. *AJR (Soc Comput Body Tomogr)* 1991;157: 616.
30. Fletcher B, Jacobstein M. MRI of congenital abnormalities of the great vessels. *AJR* 1986;146:941.
31. Utz JA, Herfkens RJ, Heinsimer JA, Shimakawa A, Glover GH, Pelc NJ. Valvular regurgitation: dynamic MR imaging. *Radiology* 1988;168:91–4.
32. Underwood S, Firmin D, Rees R, Longmore D. Magnetic resonance velocity mapping. *Clin Phys Physiol Meas* 1990; 11:37–43.
33. Vock P, Terrier F, Wegmuller H, et al. Magnetic resonance angiography of abdominal vessels: early experience using the three-dimensional phase-contrast technique. *Br J Radiol* 1991;64:10–6.
34. Enzmann D, Ross M, Marks M, Pelc N. Blood flow in major cerebral arteries as measured by phase-contrast cine MR. *Proc Soc Magn Reson Med* 1991:92.
35. Marks M, Pelc N, Enzmann D. Determination of cerebral blood flow with a phase-contrast cine MR technique: evaluation of normal and AVM patients. *Proc Soc Magn Reson Med* 1991:260.
36. Caputo G, Kondo C, Masui T, et al. Right and left lung perfusion: in vitro and in vivo validation with oblique-angle, velocity-encoded cine MR imaging. *Radiology* 1991;180: 693–8.
37. Kondo C, Caputo GR, Semelka R, Foster E, Shimakawa A, Higgins CB. Right and left ventricular stroke volume measurements with velocity encoded cine MR imaging. *AJR* 1991;157:9–16.
38. Enzmann D, Pelc N. Normal flow patterns of intracranial and spinal cerebrospinal fluid defined with phase-contrast cine MR imaging. *Radiology* 1991;178:467–74.
39. Cohen MS, Weisskoff R, Rzedzian R. Clinical methods for single-shot "instant" MR imaging of the heart. *Radiology* 1989;173P:359.
40. Meyer CH, Macovski A, Nishimura DG. Square-spiral fast imaging. *Proc Soc Magn Reson Med* 1989:362.
41. Chien D, Edelman RR. Ultrafast imaging using gradient echoes. *Magn Reson Q* 1991;7:31–56.
42. Evans AJ, Grist TM, Hedlund LW, et al. Fast MR imaging measurement of steady and pulsatile flow velocity. *Radiology* 1990;177P:201.
43. Zerhouni EA, Parish DM, Rogers WJ, Yang A, Shapiro EP. Human heart: tagging with MR imaging—a method for noninvasive assessment of myocardial motion. *Radiology* 1988; 169:59–63.
44. Axel L, Dougherty L. Heart wall motion: improved method of spatial modulation of magnetization for MR imaging. *Radiology* 1989;171:841–5.
45. Pelc NJ, Pelc LR, Herfkens RJ, Glover GH. Measurement of myocardial motion dynamics with phase contrast cine MR imaging. *Radiology* 1990;177P:171.
46. Napel S, Frayne R, Rutt BK. Computation and display of 3-D blow streamlines from 3-D phase contrast MRI. *Proc Soc Magn Reson Med* 1991:88.